MAGNETOHYDRODYNAMIC EFFECTS AT THE MAGNETOSPHERE BOUNDARY

by

Pompiliu Verzariu

Submitted to the
Faculty of the College of Arts and Sciences
of
The American University
in Partial Fulfillment of
the Requirements for the Degree of
Doctor of Philosophy
in
Physics

Signatures of Committee

Chairman

Dean of College

Date November 23, 1971

ACKNOWLEDGMENTS

The author wishes to thank Dr. M. Sugiura who suggested the MHD portion of the thesis and who supervised the entire work. I thank Dr. I. B. Strong for helpful discussions and for providing the unpublished Vela 2A and 2B data. Useful discussions with Dr. L. Libelo are also gratefully acknowledged. Mr. S. Favin assisted with computational analysis. This work was supported by the Applied Physics Laboratory/ Johns Hopkins University under contract N00017-72-C-4401 with the Department of the Navy.

TABLE OF CONTENTS

[Table of Contents Con'd]

LIST OF FIGURES

[List of Figures Con'd]

LIST OF TABLES

ABSTRACT

Interactions between the solar wind and the magnetosphere are discussed relative to the following two aspects: (a) variations in the compression of the magnetosphere responding to solar wind pressure changes; and (b) reflection and refraction of magnetohydrodynamic (MHD) waves at the boundary of the magnetosphere. Concerning (a), it is found that solar wind pressure changes and magnetic field changes at the Earth's surface are linearly correlated during magnetically quiet conditions in accordance with the theoretical expectations from the pressure balance between the solar wind plasma and the Earth's magnetic field. A constant of proportionality relating the two quantities is statistically determined. The average value for the proportionality constant agrees favorably with the theoretical value given by the Mead-Beard magnetosphere model. Magnetohydrodynamic (MHD) theory is used to study problem (b) above, namely the transmission of waves from the magnetosheath plasma into the magnetosphere under normal conditions of solar wind flow. Two cases taken as representative of magnetopause conditions in the vicinity of the subsolar point and near the dusk and/or dawn meridian, are considered. It is found that the total transmitted energy constitutes only about 1 to 2 percent of the energy flux for a distribution of isotropic incident waves. The flux transmitted into the magnetosphere from waves having an amplitude of 1 gamma (1 gamma = 10^{-5} gauss) is roughly of the order 10^{-6} to 10^{-5} erg cm^{-2} sec^{-1}. Assuming a steady isotropic flux of waves with ampli-

tudes of 1 gamma incident on a hemispherical sunward magnetospheric boundary of radius 15 R_E (earth radii), the total energy input into the magnetosphere is estimated to be of the order of 10^{21} erg per day. The wavelengths and amplitudes of the ripples induced by the MHD waves on the boundary surface are also examined. For the observed power density of MHD waves in the magnetosheath, the calculated wavelengths range from a few tenths of 1 R_E to several hundred earth radii.

1.0 INTRODUCTION

The problem of the interaction of the solar wind with the Earth's magnetosphere has been the object of considerable study over the last few decades. Many geophysical processes are connected directly or indirectly with solar phenomena, and depend on electromagnetic interactions between the solar wind and the geomagnetic field. With the advent of artificial earth satellites and space probes it became possible to carry out direct measurements in space, and a clearer picture of the near Earth environment emerged. It was discovered that the geomagnetic field is confined to a finite region, known as the magnetosphere, by the pressure of solar plasma which flows almost radially from the Sun. The solar plasma, known as the solar wind, carries weak magnetic fields imbedded in it, and as it interacts with the geomagnetic field, it causes the formation of an extremely long magnetic tail. Due to the fact that the solar wind encounters the Earth's magnetic field with a supersonic flow velocity, a collisionless bow shock is set up upstream in the wind. The gross features of the boundary between the magnetosphere and the interplanetary plasma can be adequately understood on the basis of magnetohydrodynamics.

The turbulent transition region between the collisionless bow shock and the magnetosphere boundary (magnetopause) is known as magnetosheath, and has been recognized as a region where complex electrodynamic phenomena take place. A viscous-type interaction has been proposed between the solar wind plasma and the geomagnetic field to

explain the formation of the long magnetic tail. The exact nature of this interaction is still not clear, though various hypotheses have been advanced in the published literature. In the following chapters we shall: (a) infer the existence of currents flowing at the magnetopause boundary from magnetic observations at the Earth's surface; (b) review and develop magnetohydrodynamic (MHD) relations in a form suitable for their use in the last chapter; and (c) apply the MHD relations to the reflection and transmission of waves at the magnetopause. Transmission of such waves has been proposed as a means to transport energy and momentum from the solar wind into the magnetosphere.

2.0 GEOMAGNETIC FIELD VARIATIONS CAUSED BY SOLAR WIND PRESSURE CHANGES

2.10 Introduction

The interaction of the solar wind with the magnetosphere is a complicated physical phenomenon. The principal effects of the interaction are the bow shock upstream in the wind,[1] and the overall confinement of the geomagnetic field in a comet-shaped region.[2-7] The gross features of the interaction can be adequately understood on the basis of magnetohydrodynamics.[8-11] Several models have been proposed, treating the solar wind as a conducting, field free, zero-temperature plasma incident upon a plasma-free dipole field.[12-14] The plasma is assumed to be specularly reflected from the boundary surface. Protons and electrons in the solar wind will penetrate in the boundary layer (the magnetopause) approximately one cyclotron radius, be bent in opposite directions by the Earth's magnetic field, and create a surface current. It is this current that effectively terminates the geomagnetic field and determines the shape and position of the sunward magnetopause.

The theory predicts that the field B_b at the Earth due to the boundary currents is related to the solar wind pressure P_s at the stagnation point by

$$B_b = K(P_s)^{\frac{1}{2}} \qquad (2.10\text{-}1)$$

where K is a proportionality constant. In the limit of high Mach

number that applies to the solar wind, the stagnation pressure is related to the upstream solar wind momentum flux ρV^2 by,[15]

$$P_s = \left(\frac{\gamma+1}{2}\right)^{(\gamma+1)/(\gamma-1)} (\gamma)^{-\gamma/(\gamma-1)} \rho V^2 \qquad (2.10\text{-}2)$$

where γ is the ratio of specific heats. Since $\rho = n/m$, equation (2.10-1) can be written in terms of a new constant of proportionality as

$$B_b = K_o n^{\frac{1}{2}} V \qquad (2.10\text{-}3)$$

Using a spherical harmonic description of the distorted geomagnetic field, Mead[16] calculated $K_o = 0.0305$ with n in protons/cm^3, V in km/sec and the field in gamma ($= 10^{-5}$ gauss). An experimental value for K_o has been obtained by Siscoe et al.[17] who related the size of geomagnetic sudden impulses to the associated changes in the solar wind parameters. The result supports the general functional relation expected from theory but the experimental value obtained for K_o is approximately 1/2 that predicted theoretically by Mead.[16] They tentatively attribute the discrepancy to shortcomings of the model such as the neglect of effects due to the seasonal inclination of the dipole axis, the solar wind magnetic field and the magnetospheric particle population, and conclude that these effects could, in fact, account for a large part in the discrepancy in the determination of K_o. Beard[18] indicates that the maximum seasonal effect due to the tilting of the dipole axis should be less than 10%. In a more recent paper, Ogilvie et al.,[19] using the plasma electrostatic analyzer

on Explorer 34 and magnetograms from 6 low-latitude stations, have obtained a value for K_o which is consistent with the observations of Siscoe et al.[17]

2.20 Observations

In the present paper the value of K_o is to be determined statistically by comparing solar wind data from the Vela 2A and 2B satellites with the hourly D_{st} values for the period July 1964 to July 1965.[20] The D_{st} magnetic index is defined as the disturbance field at the geomagnetic equator averaged over all longitudes, after the solar quiet daily variations, S_q, has been subtracted.[21,22] The resulting disturbance field is interpreted as being produced by the ring-current system in the magnetosphere and by currents flowing on the magnetosphere boundary. The ring-current system produces a magnetic perturbation at the Earth's surface directed so as to decrease the Earth's internal field,[23-25] the boundary current, which is associated with changes in the solar wind plasma pressure, enhances the Earth's field at low latitudes.[16] Accordingly, periods of consistently positive D_{st} (≥ 5 gamma) shall be interpreted as indicative of enhanced boundary currents corresponding to increased solar wind pressure, and periods of negative D_{st} as indicative of enhanced ring-currents.

If one makes the reasonable assumption that, during those magnetically quiet times when the D_{st} is consistently positive, the rate of change of the ring-current term, DR, is small, then one will expect to observe the linear dependence of D_{st} on changes in the solar wind

pressure. The resulting constant of proportionality will be statistically determined.

The solar wind data used was obtained by the Vela 2A and Vela 2B satellites during the period from July 1964 to July 1965. The orbits of these satellites are approximately circular with a radius of $\sim 18\ R_E$ and inclined $\sim 60°$ to the ecliptic. The satellites spend about one third of their orbit in the solar wind plasma.

Figure 1 shows three days, out of a total of 19 days, when the linear dependence was observed. Hourly averages of $n^{\frac{1}{2}}V$ are compared here with corresponding hourly values of D_{st}. The plots include measurements from both Vela 2A and 2B as indicated in the figure. Although combining the data from the two satellites would imply that the solar wind behavior is uniform over large regions of space, it is felt that, during the magnetically quiet-times under consideration, this is an acceptable assumption. Some of the scatter seen in the data may be due to the fact that the solar wind measurements are nonuniformly distributed over the hour, and quite often do not exceed three measurements during a particular hour. Note that for the three cases, as for the other 19 cases, the D_{st} level is consistently positive, indicating that the main contribution to the perturbation field at the Earth's surface during these times comes from boundary currents. Over the time span from July 1964 to July 1965, for which solar wind data were analyzed, significant changes in the background level of the data were observed, as shown in Figure 1. These changes are interpreted as being due to changes in the level of the quiet-time ring-current.

FIGURE 1.

Hourly Averages of $n^{\frac{1}{2}}V$ Plotted Against Hourly Averages of D_{st} for the Three Days Indicated

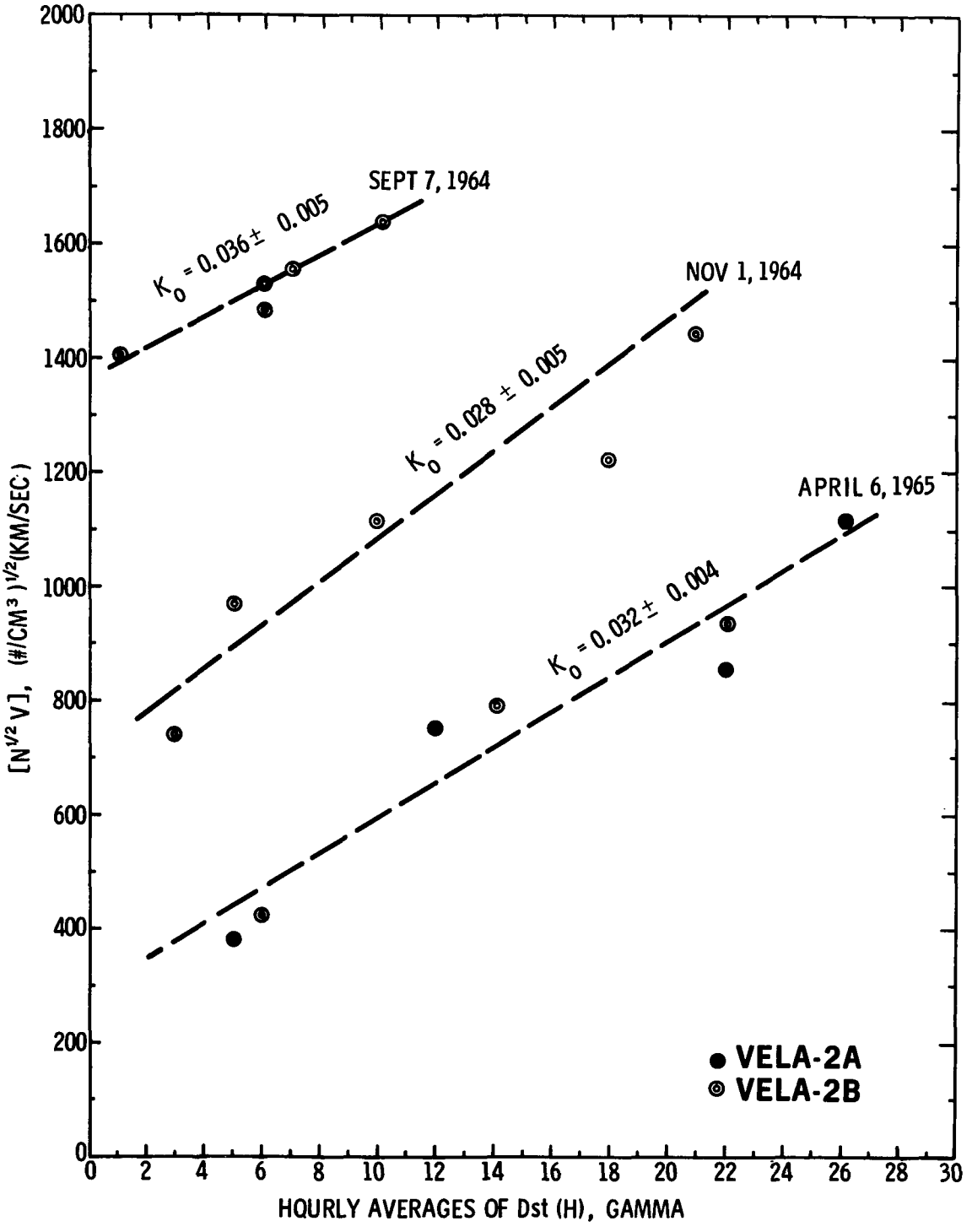
2000
1800
1600
1400
1200
1000
800
600
400
200
0
0
2
4
6
8
10
12
14
16
18
20
22
24
26
28
30
SEPT 7, 1964
$K_0 = 0.036 \pm 0.005$
NOV 1, 1964
$K_0 = 0.028 \pm 0.005$
APRIL 6, 1965
$K_0 = 0.032 \pm 0.004$
● VELA-2A
◎ VELA-2B
$[N^{1/2} V]$, $(\#/CM^3)^{1/2}(KM/SEC)$
HOURLY AVERAGES OF Dst (H), GAMMA

Figure 2 shows the results of a linear least squares fit to the 19 sets of data used in this analysis. The histogram on the left side describes the distribution of the slope K_o, while the histogram on the right side describes the distribution of the intercept K_1, the latter being the extrapolated intersection of the linear fit corresponding to zero solar wind pressure. The changes in the magnitude of K_1 are indicative of the changes in the magnitude of the ring-current field DR during these magnetically quiet periods. The upper portion of each histogram shows the average error of the quantities K_o and K_1 within the respective ranges shown on the abscissa. There is considerable spread in the distribution of the constant of proportionality. The data seem to indicate that, within the error measurement, K_o varies considerably in time, with most of its values falling below that predicted by the theoretical model of Mead.[16]

In order to combine all 19 sets of data in a single $(n^{\frac{1}{2}}V)$ vs. D_{st} plot, the following procedure was adopted:

(a) A least squares fit was made for each data set.

(b) A reference value, denoted as $(n^{\frac{1}{2}}V)^*$, was then read from each least-squares fitted curve, corresponding to the arbitrary reference value $(D_{st})^* = 15$ gamma.

(c) All data points in each set were scaled relative to their respective reference values of $(n^{\frac{1}{2}}V)^*$ and $(D_{st})^*$.

(d) The resulting differences were combined in one plot.

Figure 3 shows the combined 19 sets of data. The linear dependence in the figure is clearly apparent and the magnitude of the resulting slope

FIGURE 2.

Histograms Describing the Distributions of the Slope K_o and Intercept K_1 for 19 Sets of Data

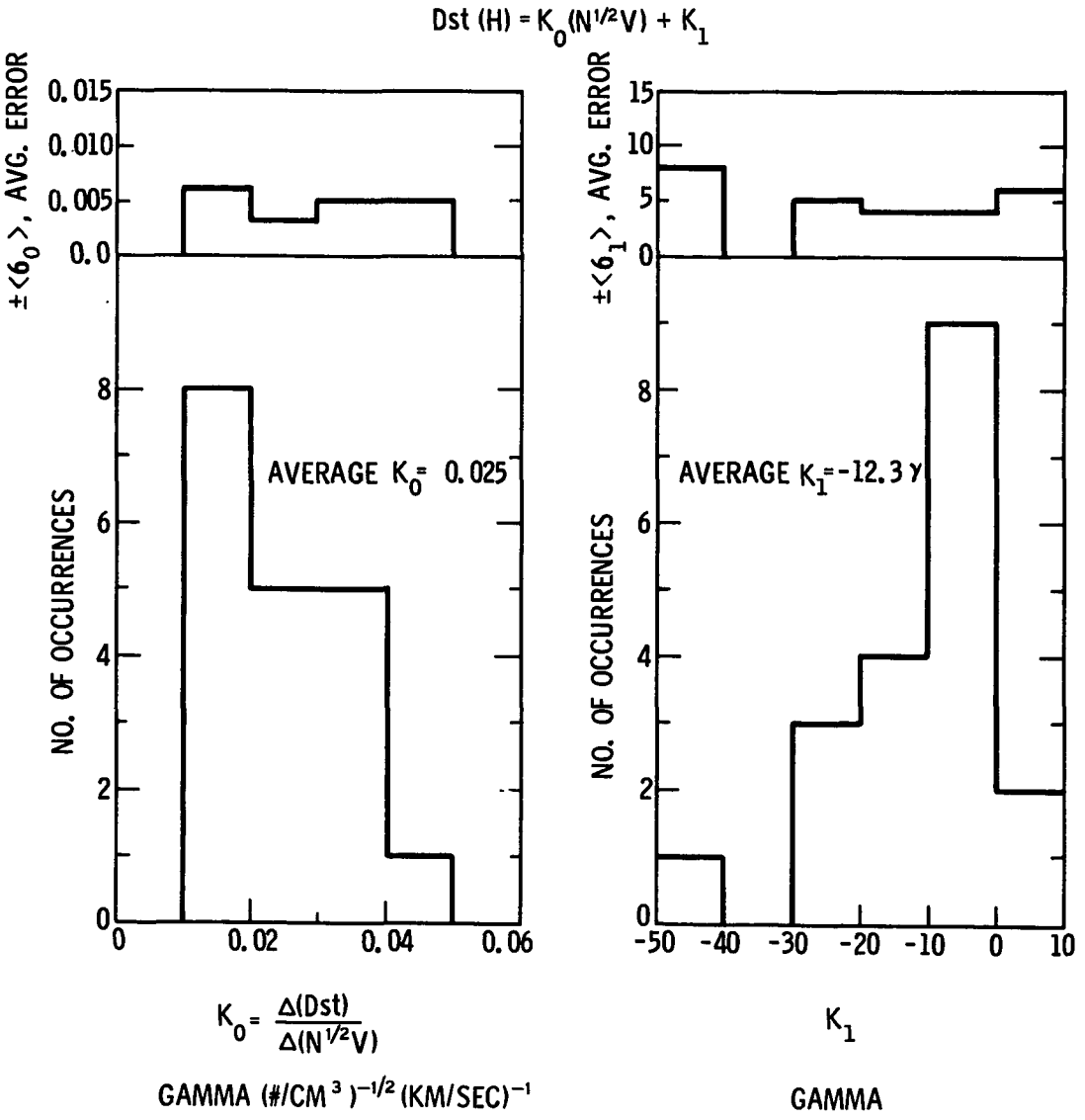
Dst (H) = $K_0(N^{1/2}V) + K_1$
$\pm\langle\sigma_0\rangle$, AVG. ERROR
0.015
0.010
0.005
0.0
NO. OF OCCURRENCES
8
6
4
2
0
AVERAGE K_0 = 0.025
0
0.02
0.04
0.06
$K_0 = \frac{\Delta(Dst)}{\Delta(N^{1/2}V)}$
GAMMA $(\#/CM^3)^{-1/2}(KM/SEC)^{-1}$
$\pm\langle\sigma_1\rangle$, AVG. ERROR
15
10
5
0
AVERAGE K_1 = -12.3 γ
-50
-40
-30
-20
-10
0
10
K_1
GAMMA

FIGURE 3.

$n^{\frac{1}{2}}V$ Against D_{st} Plot for the Combined

19 Sets of Data

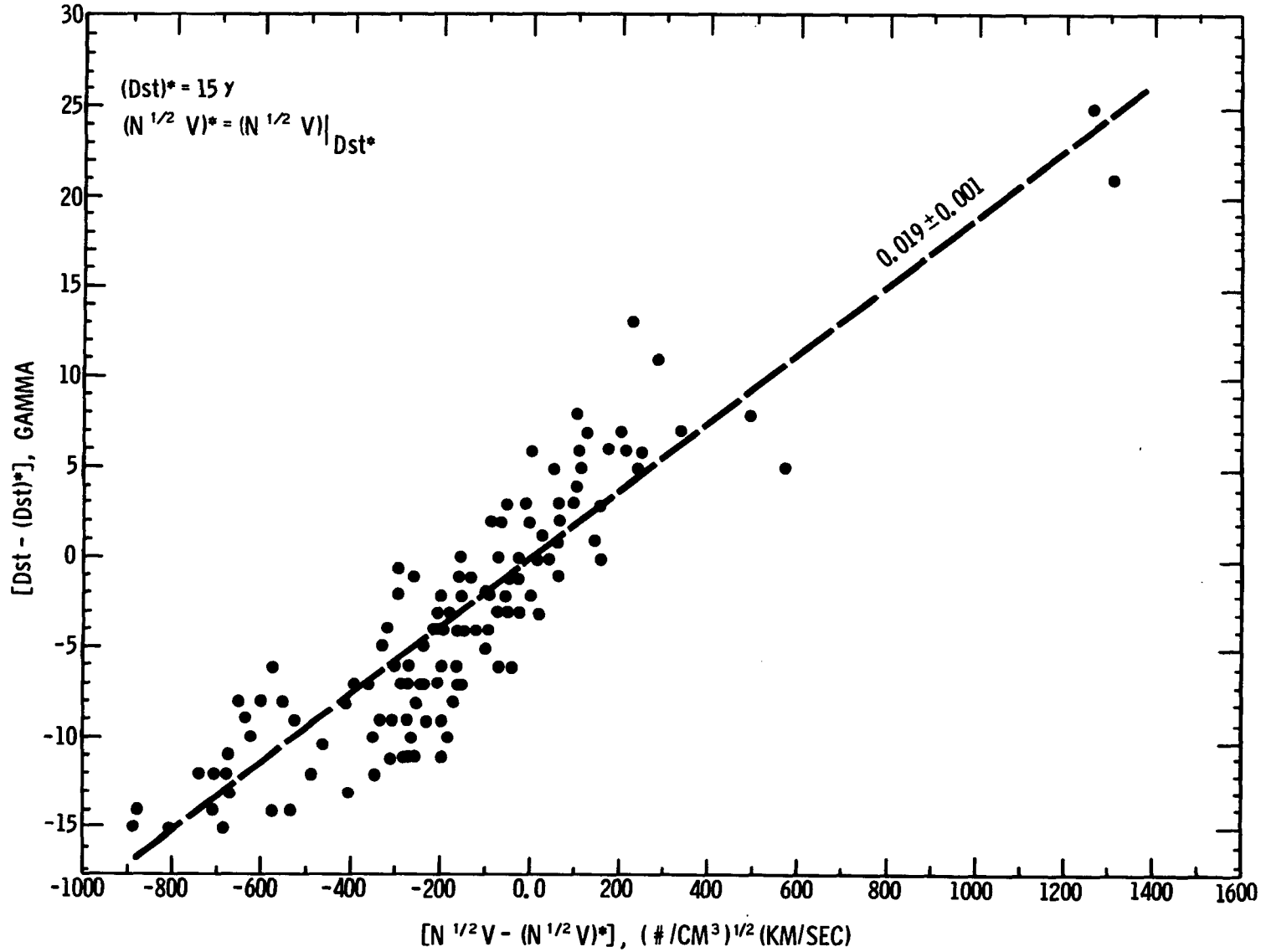
(Dst)* = 15 γ
(N 1/2 V)* = (N 1/2 V)| Dst*
0.019 ± 0.001
[Dst - (Dst)*], GAMMA
[N 1/2 V - (N 1/2 V)*], (#/CM3)1/2 (KM/SEC)
30
25
20
15
10
5
0
-5
-10
-15
-1000
-800
-600
-400
-200
0.0
200
400
600
800
1000
1200
1400
1600

(0.019 ± 0.001) is consistent with the statistical behavior of K_o over the period from July 1964 to July 1965.

2.30 The Magnetic Storm of April 17, 1965

On April 17, 1965, a sudden commencement started at 1312 UT, followed by a large geomagnetic storm. A negative impulse occurred at 1730 UT. Beginning at 1930 UT and lasting until early on April 18, the horizontal component of the magnetic field was higher than normal. The main phase decrease began sometime between 0100 and 0300 UT, reaching its maximum depression sometime between 0800 and 1100 UT on April 18. Figure 4 shows the behavior of $(n^{\frac{1}{2}}V)$ relative to D_{st} changes for April 17 and for several days following the storm. Following the early UT hours on April 18, the D_{st} drifts rapidly towards negative values and is insensitive to changes in the solar plasma pressure, as expected from the storm enhancement of the ring-current. A slow recovery period follows, during which the solar wind velocity and density maintain a consistently low level, as shown on the right hand side portion of the figure. Finally, on May 4, 1965, after more than two weeks of slow recovery, there may be an indication of a linear behavior between $n^{\frac{1}{2}}V$ and D_{st}.

2.40 Conclusions

It has been shown that, for those magnetically quiet days when the D_{st} is consistently positive and for which the rate of change of

FIGURE 4.

Behavior of $n^{\frac{1}{2}}V$ Relative to D_{st} Following

the Magnetic Storm of April 17, 1965

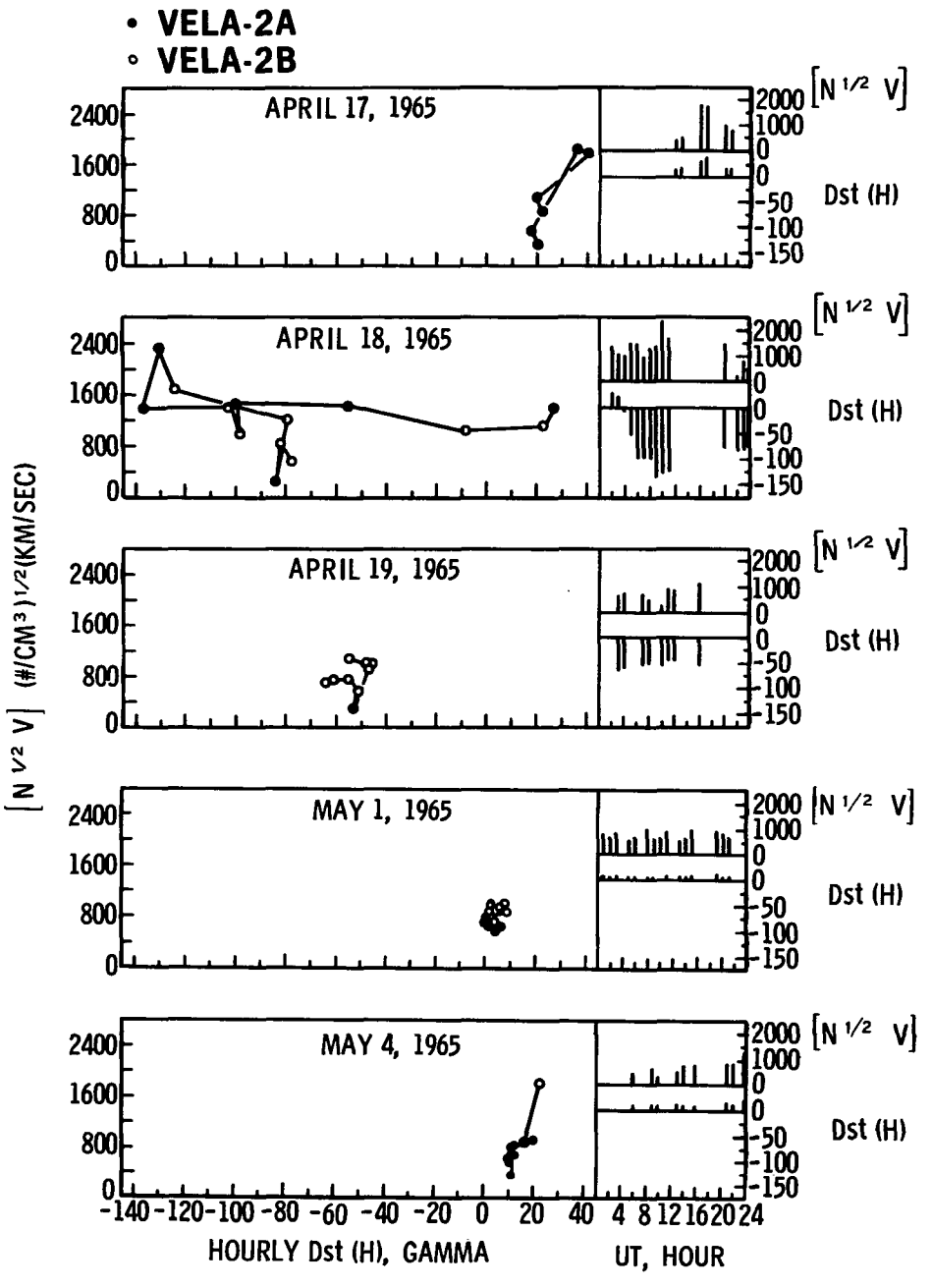
• VELA-2A
◦ VELA-2B
APRIL 17, 1965
APRIL 18, 1965
APRIL 19, 1965
MAY 1, 1965
MAY 4, 1965
[N 1/2 V] (#/CM3)1/2(KM/SEC)
[N 1/2 V]
Dst (H)
2400
1600
800
0
2000
1000
0
-50
-100
-150
-140 -120 -100 -80 -60 -40 -20 0 20 40
4 8 12 16 20 24
HOURLY Dst (H), GAMMA
UT, HOUR

the ring-current intensity is small, the changes in the D_{st} level are linearly correlated to the changes in the square root of the solar wind pressure.

The results show a considerable spread in the distribution of the constant of proportionality. The peak in the frequency distribution for this constant is in rough agreement with that obtained by Siscoe et al.[17] and Ogilvie et al.,[19] using a different technique. The average value for the proportionality constant approximately agrees with the value given by Mead.[16] Part of the discrepancy between the theoretical and experimental K_o can be attributed to the effects indicated by Siscoe et al.,[17] which were mentioned in Section 2.10, although a plot of K_o vs. month of the year (Figure 5a) does not seem to bear out a seasonal dependence. A slight dependence of K_o on the direction of flow of the solar wind with respect to the Earth-Sun axis was observed, and is shown in Figure 5b. The angles are measured in solar ecliptic coordinates.

If in addition to the protons there is a component of alpha particles in the solar plasma, with number density n_α, then the total density in equation (2.10-3) has to be written as $n = n_p + 4n_\alpha$. Since the quiet time alpha particle component in the solar wind varies between 5-10%, this correction is small. Similarly, the magnitude of K_o is quite insensitive to changes in the ratio of specific heats γ. The coefficient of ρV^2 in equation (2.10-2) varies from 0.955 for $\gamma = 1.2$, to 0.881 for $\gamma = 5/3$, and to 0.844 for $\gamma = 2$.[26] An analysis by Lees,[27] which considers the solar wind magnetic field, has the

FIGURE 5.

a) Plot of the Slope K_o Against Month of Year.

b) Plot of the Slope K_o Against Hourly Averaged Values of the Angles the Solar Wind Flow Direction Makes with the Earth-Sun Line in the Plane of the Ecliptic. Positive Angles Correspond to Flow from East of the Sun.

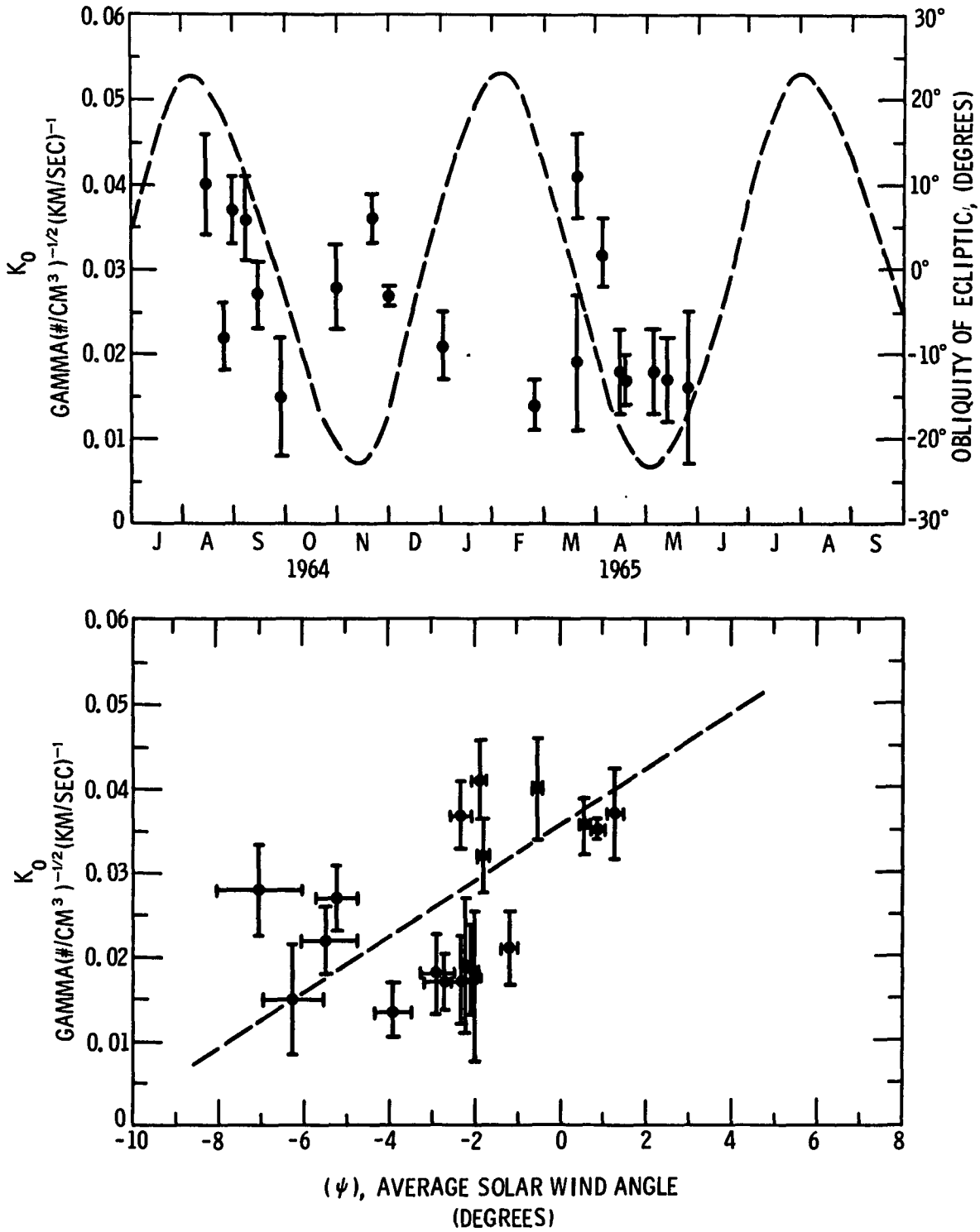
0.06
0.05
0.04
0.03
0.02
0.01
0
K_0
GAMMA(#/CM^3)$^{-1/2}$(KM/SEC)$^{-1}$
30°
20°
10°
0°
-10°
-20°
-30°
OBLIQUITY OF ECLIPTIC, (DEGREES)
J A S O N D J F M A M J J A S
1964
1965
-10 -8 -6 -4 -2 0 2 4 6 8
(ψ), AVERAGE SOLAR WIND ANGLE
(DEGREES)

coefficient of ρV^2 varying from 0.667, when the field is perpendicular to the plasma velocity, to 0.832 when parallel. For inelastic collisions at the boundary, we have $(P_s/\rho V^2) = 1.0$, while for specular reflection $(P_s/\rho V^2) = 2.0$. The changes in K_o due to the above effects amount to 3-7%. Although the individual effects discussed above might explain part of the scatter observed in the values of the constant of proportionality, the major contribution to the discrepancy between theoretical and experimental K_o is believed to be probably due to temporal changes in the magnetospheric particle population. As stated before, the present analysis assumes that the rate of change of the magnetospheric current system is negligible for the 19 cases considered. This assumption might be only approximately correct.

In conclusion, the results of the present analysis confirm the relation expected from theory between solar wind dynamic pressure and the magnetic field changes. The spread in the values of K_o, would indicate shortcomings in the theoretical model rather than experimental errors. Future study should isolate the effects of the individual factors other than solar wind pressure changes, that contribute to the variations in the magnetic field at the Earth's surface.

3.0 MAGNETOHYDRODYNAMIC THEORY

3.10 Introduction

Magnetohydrodynamics is the study of the motion of an electrically conducting fluid in the presence of a magnetic field. The ambient field acts on the electrons and ions of the medium producing dynamical effects such as bulk motion. These effects in turn couple with the ambient magnetic field and modify it. It should be noted that the fundamental equations of magnetohydrodynamics rest on the assumption that the conducting medium can be considered as a fluid. Thus to satisfy this assumption one must consider only wavelengths large enough that the plasma will act as a continuum. These low frequency oscillation involve motion of the fluid but no charge separation, so that it is customary in the magnetohydrodynamic approximation to neglect the displacement current in Ampère's law.

The theory of hydromagnetic waves has been discussed by many authors.[28-32] A compressible, nondissipative, hydromagnetic medium will propagate small amplitude plane waves at three distinct speeds corresponding to three different polarizations of the fluid displacement. One type of transmitted wave will propagate as a purely transverse disturbance, where both the fluid displacement and the magnetic disturbance are normal to the direction of propagation and to the undisturbed ambient magnetic field. This shear wave is known

as an Alfvén wave, after the physicist who predicted it theoretically.

The other two modes of propagated waves result in displacements that are coplanar with the propagation vector and the undisturbed field and involve compression that alters the thermodynamic state of the medium. These waves are known as magnetoacoustic.

The subject of magnetohydrodynamics has found application in cosmic electrodynamics and in such low-density, magnetically permeated ionized media as the magnetosphere and interplanetary space. In these regions the magnetic restoring forces are comparable to the ordinary elasticity of the ambient plasma and hydromagnetic waves can propagate.

3.20 Basic MHD Equations

We consider a nonrelativistic, perfectly conducting fluid in a homogeneous magnetic field $\bar{B}$. Dissipation resulting from the fluid viscosity and thermal conductivity as well as the displacement current and additional external force fields are neglected. Under these conditions, the equation of motion, Maxwell's equations, the continuity equation, and the equation of energy conservation become (in Gaussian units)

$$\rho \frac{d\bar{V}}{dt} = - \nabla P + \frac{1}{c} (\bar{J} \times \bar{B}) \tag{3.20-1}$$

$$\nabla \cdot \bar{B} = 0 \tag{3.20-2}$$

$$\nabla \times \bar{B} = \frac{4\pi\mu}{c} \bar{J} \tag{3.20-3}$$

$$\nabla \times \bar{E} = - \frac{1}{c} \frac{\partial \bar{B}}{\partial t} \tag{3.20-4}$$

$$\frac{d\rho}{dt} + \rho \nabla \cdot \bar{V} = 0 \tag{3.20-5}$$

$$\frac{ds}{dt} = 0 \tag{3.20-6}$$

where s is the entropy of the system and

$$\frac{d}{dt} = \frac{\partial}{\partial t} + \bar{V} \cdot \nabla \tag{3.20-7}$$

is the substantial derivative. Since we assume infinite conductivity, the requirement of finite currents presupposes that there can be no electric field in a coordinate system at rest with the fluid. This

means that in this coordinate system

$$\bar{E} + \frac{1}{c} \bar{V} \times \bar{B} = 0 \qquad (3.20\text{-}8)$$

For the compressible, isotropic plasma at hand, the continuity equation can be combined with thermodynamic relations to relate pressure and density variations

$$\frac{dP}{dt} - S^2 \frac{d\rho}{dt} = 0 \qquad (3.20\text{-}9)$$

where $S = \sqrt{\gamma P/\rho}$ is the velocity of sound and $\gamma = c_p/c_v$ is the ratio of specific heats. The set of nonlinear equations given in (3.20-1) through (3.20-6) can be simplified to a linear form by a first order perturbation scheme. It is assumed that all unperturbed quantities which characterize the medium are functions of neither space nor time. A variable X is written as $X = X_o + x_1$, where the subscript zero denotes the steady-state quantity and the subscript 1 denotes the small perturbation. Assume further that all perturbation quantities vary as

$$\exp[i(\omega t - \bar{k}\cdot\bar{r})] \qquad (3.20\text{-}10)$$

and let the amplitude of their oscillations be denoted by (ρ', v', p', etc.). Equations (3.20-1) through (3.20-6) then reduce, after some manipulation, to the following algebraic system

$$\rho_o \omega \bar{v}' = \left(p' + \frac{\bar{B}_o \cdot \bar{b}'}{4\pi\mu}\right) \bar{k} - \left(\frac{\bar{k}\cdot\bar{B}_o}{4\pi\mu}\right) \bar{b}' \qquad (3.20\text{-}11)$$

$$\bar{k}\cdot\bar{b}' = 0 \qquad (3.20\text{-}12)$$

$$\omega\bar{b}' = (\bar{k}\cdot\bar{v}')\bar{B}_o - (\bar{k}\cdot\bar{B}_o)\bar{v}' \qquad (3.20\text{-}13)$$

$$\omega\rho' - \rho_o(\bar{k}\cdot\bar{v}') = 0 \qquad (3.20\text{-}14)$$

When linearized, the isotropic condition P = const. ρ^γ, yields the following relation between the magnitudes of the perturbation pressure and density

$$p' = S^2\rho' \qquad (3.20\text{-}15)$$

so that one of the thermodynamic variables in the MHD equations can be eliminated.

3.30 Magnetoacoustic Waves

Consider the inner product of equation (3.20-11) with $\bar{k}$ and then $\bar{B}_o$, and the inner product of equation (3.20-13) with $\bar{B}_o$. Substitute (3.20-15) in (3.20-14). The four scalar equations which result can be written as

$$\begin{bmatrix} -k^2 & \rho_o\omega & \frac{-k^2}{4\pi\mu} & 0 \\ -(\bar{k}\cdot\bar{B}_o) & 0 & 0 & \rho_o\omega \\ 0 & -B_o^2 & \omega & (\bar{k}\cdot\bar{B}_o) \\ \omega & -\rho_o S^2 & 0 & 0 \end{bmatrix} \begin{bmatrix} p' \\ (\bar{k}\cdot\bar{v}') \\ (\bar{B}_o\cdot\bar{b}') \\ (\bar{B}_o\cdot\bar{v}') \end{bmatrix} = 0 \qquad (3.30\text{-}1)$$

A nontrivial solution is obtained if the determinant of equation (3.30-1) vanishes. This condition gives the following well-known dispersion relation for magnetoacoustic waves

$$\omega^4 - k^2(S^2 + A^2)\omega^2 + k^4 S^2 A^2 \cos^2\theta = 0 \qquad (3.30\text{-}2)$$

where $A = |\bar{A}| = |\bar{B}_o/\sqrt{4\pi\mu\rho_o}|$ is the Alfvén velocity, and where $\theta = \cos^{-1}(\bar{k}\cdot\bar{A}/kA)$ is the angle the wave propagation vector makes with the ambient magnetic field. The roots of equation (3.30-2) are given by

$$\frac{\omega}{k} = \frac{1}{2}[(S^2 + A^2 + 2SA\cos\theta)^{\frac{1}{2}} \pm (S^2 + A^2 - 2SA\cos\theta)^{\frac{1}{2}}] \qquad (3.30\text{-}3)$$

and the wave is termed fast or slow depending on whether the plus or minus sign is assigned to its phase velocity. Waves propagating normal to $\bar{B}_o$ will do so only in the fast mode giving rise to a compressional disturbance having phase velocity

$$\left(\frac{\omega}{k}\right)_f = \pm\sqrt{S^2 + A^2} \qquad (3.30\text{-}4)$$

while waves propagating along $\bar{B}_o$ will produce compressional and transverse disturbances having respective phase velocities

$$\left(\frac{\omega}{k}\right)_s = \pm S \qquad (3.30\text{-}5)$$

$$\left(\frac{\omega}{k}\right)_f = \pm A \qquad (3.30\text{-}6)$$

The plus or minus sign refers to waves traveling in opposite directions.

Equations (3.20-11), (3.20-13), (3.20-14) and (3.20-15) can be solved simultaneously to give the following perturbation quantities

$$\bar{v}' = \frac{\omega}{k^2 S^2}\left[\frac{\omega^2\bar{k} - k^2(\bar{k}\cdot\bar{A})\bar{A}}{\omega^2 - (\bar{k}\cdot\bar{A})^2}\right]\frac{p'}{\rho_o} \qquad (3.30\text{-}7)$$

$$\bar{b}' = \frac{\omega^2}{k^2 S^2}\left[\frac{k^2\bar{B}_o - (\bar{k}\cdot\bar{B}_o)\bar{k}}{\omega^2 - (\bar{k}\cdot\bar{A})^2}\right]\frac{p'}{\rho_o} \qquad (3.30\text{-}8)$$

It can be seen that these perturbation vectors will be confined to the plane defined by the propagation vector $\bar{k}$ and the undisturbed magnetic field $\bar{B}_o$.

3.40 Alfvén Waves

Alfvén waves will propagate along the field independently on whether the fluid is compressible or incompressible. This can be seen by setting $\rho' = 0$ in equation (3.20-14). Then $(\bar{k}\cdot\bar{v}') = 0$, and if the inner product of equation (3.20-11) with $\bar{k}$ is taken and (3.20-15) is used, it follows that $(\bar{B}_o\cdot\bar{b}') = 0$. With these results, equations (3.20-11) and (3.20-13) become

$$\omega\bar{v}' + \frac{(\bar{k}\cdot\bar{B}_o)}{4\pi\mu\rho_o}\bar{b}' = 0 \qquad (3.40\text{-}1)$$

$$(\bar{k}\cdot\bar{B}_o)\bar{v}' + \omega\bar{b}' = 0 \qquad (3.40\text{-}2)$$

Solving the above equations simultaneously we obtain

$$\frac{\omega}{k} = \pm\frac{B_o}{\sqrt{4\pi\mu\rho_o}}\cos\theta \qquad (3.40\text{-}3)$$

which is the phase velocity of Alfvén waves, and conforms to the conception of oscillations propagating along the field lines. The plus or minus sign in equation (3.40-3) corresponds to waves propagating along or opposite the direction of $\bar{B}_o$. The properties $(\bar{k}\cdot\bar{b}') = (\bar{B}_o\cdot\bar{b}') = 0$

show that these waves are transverse to both the direction of propagation and the direction of the magnetic field. Their disturbance vector rotates about the undisturbed direction of the ambient lines of force.

3.50 Group Velocity

The group velocity with which MHD waves propagate can be obtained from the formula

$$\bar{v}_g = \frac{\partial \omega}{\partial \bar{k}} \tag{3.50-1}$$

We can write equations (3.30-2) and (3.40-3) as

$$\omega^4 - \bar{k}\cdot\bar{k}(S^2 + A^2)\omega^2 + \bar{k}\cdot\bar{k}S^2(\bar{k}\cdot\bar{A})^2 = 0 \tag{3.50-2}$$

$$\omega = \pm (\bar{k}\cdot\bar{A}) \tag{3.50-3}$$

Differentiating the above equations according to (3.50-1) we obtain

Alfvén wave:
$$\bar{v}_g = \pm \bar{A} \tag{3.50-4}$$

Magnetoacoustic wave:
$$\bar{v}_g = \frac{\omega^4\bar{k} - k^4S^2(\bar{k}\cdot\bar{A})\bar{A}}{\omega k^2[2\omega^2 - (S^2 + A^2)k^2]} \tag{3.50-5}$$

3.60 Energy Density and Flux

Conservation of energy requires that

$$\frac{\partial E}{\partial t} + \nabla\cdot\bar{F} = 0 \tag{3.60-1}$$

where E is the energy density and $\overline{F}$ is the energy flux of MHD waves

$$E = \rho(U + \frac{V^2}{2}) + \frac{B^2}{8\pi\mu} \tag{3.60-2}$$

$$\overline{F} = \rho\overline{V}(H + \frac{V^2}{2}) + \frac{B^2}{4\pi\mu}\overline{V} - \frac{\overline{B}\cdot\overline{V}}{4\pi\mu}\overline{B} \tag{3.60-3}$$

Here U is the internal energy per unit mass and H is the enthalpy per unit mass. With the help of equations (3.20-1) through (3.20-5) equation (3.60-2) can be manipulated into the form

$$\frac{dU}{dt} + P\frac{d}{dt}(\frac{1}{\rho}) = T\frac{ds}{dt} = 0 \tag{3.60-4}$$

which checks with equation (3.20-6) and shows that because dissipation has been neglected, the entropy of the system remains constant.

In the following presentation we shall follow a treatment described by Anderson.[33] Let each variable be written as before in the form, e.g. $\rho = \rho_o + \rho_1$ and consider the following expansions

$$\rho U = (\rho U)_o + \frac{\partial(\rho U)}{\partial\rho}\Big|_o \rho_1 + \frac{1}{2}\frac{\partial^2(\rho U)}{\partial\rho^2}\Big|_o \rho_1^2 + \cdots$$

$$= (\rho U)_o + H_o\rho_1 + \frac{1}{2}(\frac{S^2}{\rho})_o \rho_1^2 + \cdots$$

$$\frac{1}{2}\rho V^2 = \frac{1}{2}(\rho_o + \rho_1)(\overline{V}_o + \overline{V}_1)^2$$

$$\frac{B^2}{8\pi\mu} = \frac{1}{8\pi\mu}(\overline{B}_o + \overline{b}_1)^2$$

$$H = H_o + (\frac{\partial H}{\partial\rho})_s \rho_1 + \cdots = H_o + (\frac{S^2}{\rho})\rho_1 + \cdots$$

$$\overline{B}\cdot\overline{V} = (\overline{B}_o + \overline{b}_1)\cdot(\overline{V}_o + \overline{v}_1)$$

The perturbation quantities are assumed to be proportional to $\exp[i(\omega t - \bar{k}\cdot\bar{r})]$. If time averages of the above expansions are considered, only those terms where the oscillatory quantities appear as a square will have a non-zero mean and will therefore contribute to the energy density or flux of the wave. Preserving only first-order terms, and substituting the above expansions in equations (3.60-2) and (3.60-3), we obtain the following relations for the perturbation amplitudes

$$\langle E' \rangle = \frac{1}{2}\left[\frac{1}{2}\frac{S^2}{\rho_o}\rho'^2 + \frac{1}{2}\frac{b'^2}{4\pi\mu} + \frac{1}{2}\rho_o v'^2\right] \tag{3.60-5}$$

$$\langle \bar{F}' \rangle = \frac{1}{2}\rho_o\left[\frac{S^2}{\rho_o}\rho'\bar{v}' + 2\frac{(\bar{B}_o\cdot\bar{b}')}{4\pi\mu\rho_o}\bar{v}' - \frac{(\bar{B}_o\cdot\bar{v}')}{4\pi\mu\rho_o}\bar{b}' - \frac{(\bar{b}'\cdot\bar{v}')}{4\pi\mu\rho_o}\bar{B}_o - \frac{B_o^2}{4\pi\mu\rho_o^2}\rho'\bar{v}' + \frac{\rho'}{\rho_o}\frac{(\bar{B}_o\cdot\bar{v}')}{4\pi\mu\rho_o}\bar{B}_o\right] \tag{3.60-6}$$

With the help of equations (3.30-2), (3.30-7) and (3.30-8), we have

$$\frac{1}{2}\rho_o v'^2 = \frac{1}{2}\left(\frac{S^2}{\rho_o}\rho'^2 + \frac{b'^2}{4\pi\mu}\right) = \frac{1}{2}\left[\frac{\omega^4 - k^2S^2(\bar{k}\cdot\bar{A})^2}{\omega^2 - (\bar{k}\cdot\bar{A})^2}\right]\frac{\rho'^2}{\rho_o k^2} \tag{3.60-7}$$

thus showing equipartion between kinetic energy and the sum of magnetic and pressure energy of the magnetoacoustic wave. Substituting equation (3.60-7) in (3.60-5) and using the identity derived from (3.30-2)

$$\omega^4 - k^2S^2(\bar{k}\cdot\bar{A})^2 = 2\omega^4 - \omega^2k^2(S^2 + A^2) \tag{3.60-8}$$

we obtain

$$\langle E' \rangle = \frac{1}{2}\left[\frac{2\omega^2 - k^2(S^2 + A^2)}{\omega^2 - (\bar{k}\cdot\bar{A})^2}\right]\frac{\omega^2\rho'^2}{k^2\rho_o} \tag{3.60-9}$$

In the same way, taking the inner product of the terms shown in the expression for the energy flux, one can show, after some straightforward manipulation, that

$$\langle \bar{F}' \rangle = \frac{1}{2}\left[\frac{\omega^4\bar{k} - k^4S^2(\bar{k}\cdot\bar{A})\bar{A}}{\omega^2 - (\bar{k}\cdot\bar{A})^2}\right]\frac{\omega\rho'^2}{k^4\rho_o} \tag{3.60-10}$$

The velocity of energy propagation of small-amplitude waves is then simply

$$\bar{v}_g' = \frac{\langle \bar{F}' \rangle}{\langle E' \rangle} = \frac{\omega^4\bar{k} - k^4S^2(\bar{k}\cdot\bar{A})\bar{A}}{\omega k^2[2\omega^2 - (S^2 + A^2)k^2]} \tag{3.60-11}$$

which is the same expression derived in equation (3.50-5) for the group velocity of magnetoacoustic waves.

For Alfvén waves, we have $\rho' = (\bar{B}_o\cdot\bar{b}') = (\bar{k}\cdot\bar{v}') = 0$ and $\bar{v}' = \pm\,\bar{b}'/\sqrt{4\pi\mu\rho_o}$. Equations (3.60-5) and (3.60-6) reduce then to

$$\langle E' \rangle = \frac{b'^2}{8\pi\mu} \tag{3.60-12}$$

$$\langle \bar{F}' \rangle = \pm\frac{b'^2}{8\pi\mu}\bar{A} \tag{3.60-13}$$

Hence we have

$$\bar{v}_g' = \frac{\langle \bar{F}' \rangle}{\langle E' \rangle} = \pm\,\bar{A} \tag{3.60-14}$$

which again checks with the result previously derived in equation (3.50-4).

4.0 REFLECTION AND REFRACTION OF HYDROMAGNETIC WAVES AT THE MAGNETOPAUSE

4.10 Introduction

Over the past few years, considerable attention has been directed to energy transfer processes between the solar wind plasma and the Earth's magnetosphere. A general boundary interaction analysis should allow for diffusion of both plasma and magnetic field through the boundary region, since the merging of the interplanetary field lines with the Earth's field is believed to be an important mechanism to explain storm time geomagnetic phenomena.[34,35] However, the complete theoretical problem may well prove to be unsolvable in its complexity, while, on the other hand, the macroscopic behavior of the quiet time magnetopause has been adequately inferred from the equilibrium condition associated with the MHD pressure balance across an idealized surface.[8-14]

Finite thickness boundary layer analyses have been performed recently by Newcomb[36] and Faye-Petersen and Heckman.[37] Their viscous-like interaction is based on a pressure tensor perturbation associated with a perturbation in the ion cyclotron orbit. Eviatar and Wolf[38] propose a two-stream cyclotron instability to account for viscous transfer of energy at the magnetopause.

A viscous-like interaction of hydromagnetic waves with the magnetopause has been proposed by Axford[39] as a means to transport energy and momentum from the solar wind to the magnetosphere. The specific

mechanism invoked is the refraction of turbulent sound waves originating in the solar wind plasma which can exert transverse stresses on the magnetopause and contribute to the formation of the geomagnetic tail. The presence of a turbulent spectrum of hydromagnetic waves in the magnetosheath has been observed.[40,41] This has been attributed to the amplification of the noise spectrum in the solar wind on passage through the bow shock. Kelvin-Helmholtz instability of the magnetopause, if it occurs, would enhance the viscous interaction between the solar wind and the surface of the magnetosphere, and would thus provide a very effective, additional drag mechanism. The stability problem of the hydromagnetic Kelvin-Helmholtz model of the interface has been treated in detail in the literature,[42-51] and is discussed in the next section.

Fejer[52] has studied the theoretical problem of reflection and refraction of hydromagnetic waves at a stable, plane interface which separates two compressible, perfectly conducting media in relative motion to each other. He assumes the relative motion to be parallel to the interface and that the magnetic fields on both sides of the boundary are parallel to the boundary surface. Such a model is thought to approximate quite well the boundary between the sunward Earth's magnetosphere and the solar wind, especially during magnetically quiet times. McKenzie[51] expands Fejer's treatment to obtain values for the reflection coefficient in the following approximations: (a) the sound speed $\gg$ Alfvén speed in the solar wind; (b) the Alfvén speed $\gg$ sound speed in the magnetosphere. The conclusion reached by McKenzie is that, during quiet times, the magnetopause behaves like

a near perfect reflector to the turbulent hydromagnetic waves in the magnetosheath, and thus, the mechanism invoked by Axford[39] is not very effective, at least under normal conditions, in producing a viscous-like interaction.

In the present analysis, reflection and refraction coefficients at a stable interface are obtained as ratios of the normal components of hydromagnetic energy flux. The resulting expressions are evaluated exactly for representative conditions for the magnetopause. The momentum flux of the MHD waves refracted in the magnetosphere as well as the amplitude and wavelength of the oscillations experienced by the perturbed boundary are then calculated.

Before proceeding with the theoretical calculations we describe typical properties of the solar wind, the magnetosheath and the outer magnetosphere. Extensive observations of the magnetic field and plasma characteristics of these regions have been made by satellites and space probes.[2-7,53-66] Table 1 summarizes typical values of plasma and magnetic parameters of the sunward magnetosheath and the outer magnetosphere for quiet conditions of the solar wind.

4.20 Instabilities

A thorough study of plasma instability processes is beyond the scope of this work. We shall briefly discuss several types of instabilities which have been suggested as pertinent to the magnetopause or microscopic, according to the frequency range of the process. The former are low-frequency phenomena and are studied using the hydromagnetic equations.

TABLE 1

A Summary of Typical Plasma and Magnetic Properties
in the Solar Wind and the Sunward Magnetopause Region for Quiet Conditions

	Outer Magnetosphere	Magnetosheath	Solar Wind
Density (cm^{-3})	0.1 - 1	10 - 35	0.3 - 10
Magnetic Field (gamma = 10^{-5} gauss)	20 - 60	10 - 40	2 - 10
Temperature (°K)	$\sim 10^4$ - 10^5	$\sim 10^5$ - 10^6	6×10^5 - 1×10^5
Bulk Velocity (km/sec)	———	0 - 3×10^2	3.5×10^2 - 4.5×10^2
Sound Speed (km/sec)	10 - 40	40 - 4×10^2	30 - 40
Alfvén Speed (km/sec)	4×10^2 - 1.3×10^3	40 - 2×10^2	10 - 56
Proton Gyro Frequency (hertz)	3×10^{-1} - 9×10^{-1}	2×10^{-1} - 6×10^{-1}	3×10^{-2} - 1.5×10^{-1}
Electron Gyro Frequency (hertz)	6×10^2 - 2×10^3	4×10^2 - 1×10^3	6×10^1 - 3×10^2

Examples are interchange, Raleigh-Taylor and Kelvin-Helmholtz instabilities. The latter are high-frequency phenomena which result from non-Maxwellian velocity distributions in the plasma. Examples are two-stream, mirror and loss-cone instabilities.

Unstable conditions at the magnetopause boundary have been proposed as a means to transfer energy from the shocked solar wind plasma to the magnetosphere. Eviatar and Wolf[38] have invoked a two-stream cyclotron instability on the flanks of the magnetosphere to account for viscous interaction at the magnetopause. Another form of plasma instability that may occur is the Rayleigh-Taylor instability. This instability was originally studied for the case of a heavy fluid supported by a light fluid in a gravitational field.[46] Still another type of instability is the one that produces waves on water when wind blows over it, and is known as the Kelvin-Helmholtz instability. Helmholtz observed that the discontinuity surface between two perfect-fluid media in relative motion effectively curls up and breaks into vortex filaments under the influence of viscous friction. The regime of Kelvin-Helmholtz instability has been studied by several authors. Stuart[42] and Lock[43] found that the presence of a magnetic field, either co-planar or perpendicular to the velocity discontinuity surface between perfectly conducting fluids, will inhibit the instability growth. Fejer[47] and Sen[48] studied the stability of a simplified model having identical acoustic and magnetic properties on either side of the boundary. Their results therefore do not seem applicable to conditions at the magnetopause. Fejer, in the cases he studied showed that the introduction of

a slight compressibility would reduce the stabilizing effect of the magnetic field, and that the first unstable modes would propagate parallel to the streaming velocity. Sen found that the most unstable perturbations propagate perpendicular to the unperturbed ambient magnetic field. Lerche[49] examined the stability question in the hydromagnetic approximation to show that the highest growth rate of unstable waves occurs for the shortest wavelengths. He therefore argued that the Vlasov equation should be employed rather than MHD theory and that, Landau damping might be effective in inhibiting the instability. Southwood[50] concluded from his analysis that, at the middle and low latitudes which are removed from the subsolar points, the first growing modes would propagate across the Earth's field. These modes exhibit nearly circular polarization in a plane almost perpendicular to the geomagnetic field. In a more recent paper, McKenzie[51] found that, during relatively quiet conditions of the solar wind, the magnetopause is unlikely to undergo Kelvin-Helmholtz instability.

At present it appears that the strongly compressed geomagnetic field on the sunward surface of the magnetosphere boundary will exert a stabilizing effect on the Kelvin-Helmholtz instability, so that, under quiet conditions of the solar wind, energy transfer due to this instability across the sunward magnetopause is likely to be negligible. The situation becomes considerably more complicated along the flanks of the magnetosphere and the magnetotail, where the dynamic pressure of the solar wind decreases. In this region the development of un-

stable regimes may be possible, especially under disturbed conditions of the solar wind.

4.30 Theory

In the following sections the MHD relations which were developed in Chapter 3.0 are applied to the problem of reflection and transmission of waves across a stable, plane boundary.

4.31 Boundary Conditions

Consider two compressible, perfectly conducting media separated by a plane boundary. In the hydromagnetic frequency range, i.e. well below the gyrofrequency of ions, a fully ionized gas may be adequately represented by an inviscid, conducting fluid. The relative motion of the fluids along the plane of the interface requires that the undisturbed, uniform magnetic field $\overline{B}$, which is assumed to have different values in the two regions, be tangential to the interface. Solutions are sought for the amplitude of the reflected and transmitted waves resulting from a small amplitude incident wave in one of the media. Let the wave solutions be proportional to $\exp[i(\omega t-\overline{k}\cdot\overline{r})]$. The restriction that the normal component of $\overline{B}$ should vanish at the boundary allows to consider the reflection and refraction of only magnetoacoustic waves since Alfvén waves will propagate along the interface without penetrating in the other medium.

The boundary conditions to be satisfied at the interface are: (a) pressure balance; (b) zero normal components of the magnetic field and the velocity; (c) matching of the tangential components of the

wave vectors. Each boundary condition shall be discussed in turn.

The pressure balance in the unperturbed state requires that

$$P_1 + \frac{B_{01}^2}{8\pi\mu} = P_2 + \frac{B_{02}^2}{8\pi\mu} \tag{4.31-1}$$

and assuming adiabatic conditions so that $P = \text{const.}\ \rho_o^{\gamma}$, one obtains

$$\rho_{01}(\gamma^{-1}S_1^2 + \tfrac{1}{2}A_1^2) = \rho_{02}(\gamma^{-1}S_2^2 + \tfrac{1}{2}A_2^2) \tag{4.31-2}$$

where S and A are the sound and Alfvén speeds respectively, and γ is the ratio of the specific heats. In the perturbed state the stress associated with the disturbance must be equal on each side. To find an expression for this stress, consider the combination of Maxwell's equations and equations of fluid dynamics, as developed in Chapter 3.0.

$$\rho_o\omega\bar{v}' = \left(p' + \frac{\bar{B}_o\cdot\bar{b}'}{4\pi\mu}\right)\bar{k} - \left(\frac{\bar{k}\cdot\bar{B}_o}{4\pi\mu}\right)\bar{b}' \tag{4.31-3}$$

$$\bar{k}\cdot\bar{b}' = 0 \tag{4.31-4}$$

$$\omega\bar{b}' = (\bar{k}\cdot\bar{v}')\bar{B}_o - (\bar{k}\cdot\bar{B}_o)\bar{v}' \tag{4.31-5}$$

$$\omega\rho' - \rho_o(\bar{k}\cdot\bar{v}') = 0 \tag{4.31-6}$$

$$p' = S^2\rho' \tag{4.31-7}$$

Here the primed quantities denote the amplitude of the perturbations. Taking the inner product of equation (4.31-3) with $\bar{k}$ and using equations (4.31-4), (4.31-6) and (4.31-7), it can be shown that

$$\left(p' + \frac{\bar{B}_o \cdot \bar{b}'}{4\pi\mu}\right) = \left(\frac{\omega/k}{S}\right)^2 p' \qquad (4.31\text{-}8)$$

where the term on the left hand side is the sum of the dynamic and magnetic perturbation pressures. Denoting the incident, reflected and transmitted quantities by the subscripts i, r, t respectively, the following expression for the pressure balance of the perturbation stress holds

$$\left(\frac{\omega_1/k_1}{S_1}\right)^2 (p_i' + p_r') = \left(\frac{\omega_2/k_2}{S_2}\right)^2 p_t' \qquad (4.31\text{-}9)$$

Assume, by virtue of linearity, that the magnetoacoustic wave impinging on the interface gives rise to a distortion which is of the same form as the incident plane wave and has amplitude δ_o

$$\delta(\bar{r},t) = \delta_o \exp[i(\omega t - \bar{k}\cdot\bar{r})] \qquad (4.31\text{-}10)$$

The vectors $\bar{k}$ and $\bar{r}$, which define the spatial distortion of the tangential discontinuity, will lie in the plane of the interface. Without loss of generality one can take region (2) to be at rest and let the plasma in region (1) flow along the interface with velocity $\bar{u}$. The boundary conditions requiring that the normal velocity and the normal magnetic field be zero on both sides of the discontinuity, are

$$v_{ni}' + v_{nr}' - \bar{u}\cdot\nabla\delta - \frac{\partial\delta}{\partial t} = v_{nt}' - \frac{\partial\delta}{\partial t} = 0 \qquad (4.31\text{-}11)$$

$$b_{ni}' + b_{nr}' - \bar{B}_{01}\cdot\nabla\delta = b_{nt}' - \bar{B}_{02}\cdot\nabla\delta = 0 \qquad (4.31\text{-}12)$$

Substituting equations (4.31-5) and (4.31-10) in equations (4.31-11) and (4.31-12) yields

$$\frac{v'_{ni} + v'_{nr}}{\omega_1} = \frac{v'_{nt}}{\omega_2} \tag{4.31-13}$$

in which $\omega_2 = \omega_1 + \bar{u}\cdot\bar{k}_1$ is the Doppler shifted frequency observed in the frame of reference stationary in region (2).

Finally, the condition that the tangential components of the wave vectors be continuous across the interface requires that

$$\omega_1 t - \bar{k}_{\ell i}\cdot\bar{r}_1 = \omega_1 t - \bar{k}_{\ell r}\cdot\bar{r}_1 = \omega_2 t - \bar{k}_{\ell t}\cdot\bar{r}_2 \tag{4.31-14}$$

Here $\bar{k}_\ell$ is the tangential component of $\bar{k}$ associated with the incident, reflected and transmitted waves as indicated in equation (4.31-14) by the appropriate subscripts. The moving reference frame in region (1) is related to the stationary frame in region (2) by the Galilean transformation

$$\bar{r}_1 = \bar{r}_2 - \bar{u}t \tag{4.31-15}$$

Substitution of equation (4.31-15) into equation (4.31-14) yields

$$k_{\ell i} = k_{\ell r} = k_{\ell t} \equiv k_\ell \tag{4.31-16}$$

$$\omega_2 = \omega_1 + \bar{u}\cdot\bar{k}_\ell \tag{4.31-17}$$

Equation (4.31-16) is the well-known Snell's law, while equation (4.31-17) is the previously derived Doppler shifted frequency in region (2).

In general, for $\bar{B}\cdot\bar{n} \neq 0$ at the boundary, a single type of wave (slow or fast) may gives rise to three different non-evanescent types of reflected and refracted waves,[67] as determined by the roots of the dispersion relation. Whenever Snell's law applies, each type of transmitted wave will propagate at an angle defined by the magnitude of the components of its refracted wave vectors. The absence of a normal component of the magnetic field at the boundary simplifies the problem considerably. This condition allows to consider only magnetoacoustic waves and to write their dispersion relation in either medium as a quadratic rather than a quartic in k_n (since $\bar{k}_n\cdot\bar{A} = 0$)

$$k_n^2 = -k_\ell^2 + \frac{\omega^4}{\omega^2(S^2+A^2)-S^2(\bar{k}_\ell\cdot\bar{A})^2} \qquad (4.31\text{-}18)$$

in terms of the parameters that define the medium and the conserved quantity $\bar{k}_\ell$. Thus the angles of reflection and refraction can be uniquely determined for a given incident wave.

It is clear that in region (2), k_{nt}^2 can acquire only real, but not necessarily positive, values. If k_{nt}^2 is negative, then the transmitted wave is evanescent and total reflection takes place. For $k_{nt}^2 > 0$, the sign of k_{nt} is chosen so as to ensure that the wave energy flux diverges from the interface.

4.32 Reflection and Transmission Coefficients

Define the reflection coefficient R as the ratio of the time averaged normal component of the reflected energy flux to that of the

incident energy flux:

$$R = \left| \frac{\langle F'_{nr} \rangle}{\langle F'_{ni} \rangle} \right| \tag{4.32-1}$$

where

$$\langle \bar{F}' \rangle = \frac{1}{2} \left[\frac{\omega^4 \bar{k} - k^4 S^2 (\bar{k} \cdot \bar{A}) \bar{A}}{\omega^2 - (\bar{k} \cdot \bar{A})^2} \right] \frac{\omega p'^2}{k^4 S^4 \rho_o} \tag{4.32-2}$$

was the expression derived in Chapter 3.0. In the same chapter, the amplitude of the perturbation velocity was found to be

$$\bar{v}' = \left[\frac{\omega^2 \bar{k} - k^2 (\bar{k} \cdot \bar{A}) \bar{A}}{\omega^2 - (\bar{k} \cdot \bar{A})^2} \right] \frac{\omega p'}{k^2 S^2 \rho_o} \tag{4.32-3}$$

Consider the inner product of equation (4.32-3) with the unit vector $\bar{n}$ normal to the boundary surface. The following relations then hold

$$\frac{v'_{nr}}{v'_{ni}} = - \frac{p'_r}{p'_i} \tag{4.32-4}$$

$$\frac{v'_{nt}}{v'_{ni}} = \frac{\omega_2}{\omega_1} \left(\frac{\omega_2/k_2}{S_2} \right)^2 \left(\frac{\omega_1/k_1}{S_1} \right)^{-2} \left[\frac{\omega_1^2 - (\bar{k}_1 \cdot \bar{A}_1)^2}{\omega_2^2 - (\bar{k}_2 \cdot \bar{A}_2)^2} \right] \frac{\rho_{01} k_{nt} p'_t}{\rho_{02} k_{ni} p'_i} \tag{4.32-5}$$

where the negative sign in equation (4.32-4) stems from the requirement that $k_{nr} = - k_{ni}$. Substituting the boundary conditions (4.31-9) and (4.31-13) together with equation (4.32-4) in equation (4.32-5), yields

$$\frac{1 - v'_{nr}/v'_{ni}}{1 + v'_{nr}/v'_{ni}} = \frac{1 + p'_r/p'_i}{1 - p'_r/p'_i} = \left[\frac{\omega_2^2 - (\bar{k}_2 \cdot \bar{A}_2)^2}{\omega_1^2 - (\bar{k}_1 \cdot \bar{A}_1)^2} \right] \frac{\rho_{02} k_{ni}}{\rho_{01} k_{nt}} \equiv Z \tag{4.32-6}$$

Using equation (4.31-2), the parameter Z can be expressed as

$$Z = \frac{k_{ni}}{k_{nt}} \left(\frac{k_2}{k_1} \right)^2 \left(\frac{\gamma^{-1} + \frac{1}{2} q_1^2}{\gamma^{-1} + \frac{1}{2} q_2^2} \right) \left(\frac{W_2^2 - q_2^2 \cos^2\theta_2}{W_1^2 - q_1^2 \cos^2\theta_1} \right) \tag{4.32-7}$$

where $W = (\omega/kS)$, and $q = (A/S)$. Whenever Snell's law applies, that is when the waves are nonevanescent ($k^2 > 0$) and are obliquely incident to the boundary surface ($k_n \neq k$), an incidence angle α_1 and a refracted angle α_2 can be defined such that

$$\frac{k_{ni}}{k_{nt}} \left(\frac{k_2}{k_1} \right)^2 = \frac{\sin 2\alpha_1}{\sin 2\alpha_2} \tag{4.32-8}$$

The magnitude of the reflection coefficient can be expressed in terms of the dimensionless parameter Z, as follows

$$R = \left(\frac{p_r'}{p_i'} \right)^2 = \left(\frac{v_{nr}'}{v_{ni}'} \right)^2 = \left(\frac{1 - Z}{1 + Z} \right)^2 \tag{4.32-9}$$

It is interesting to observe that, for particular angles of incidence and streaming velocity, the value of R can exceed unity and approach resonance as Z approaches minus one. This can occur if the flow velocity in region (1) is supersonic so that the transmitted energy, as seen from region (2) could become negative. This phenomenon, by which the energy of the medium is lower (negative) in the presence of a perturbing wave than in the absence of the wave is well known in plasma physics and is encountered in nonequilibrium transparent media which exhibit anomalous dispersion[68] and other instances in which the sign

of the energy depends on the coordinate system.[69,70] Amplified reflection of sound waves have been discussed by Miles[71] and Ribner.[72] This resonance phenomenon can be understood by chosing a coordinate system in which the pressure balance across the interface is satisfied only for a vanishingly weak incoming perturbation. In this coordinate system reflected and transmitted waves are self-excited and, in the absence of a damping mechanism, amplification is effectively infinite.

4.33 Continuity of the Normal Component of Energy Flux at the Boundary

To show that the normal energy flux is continuous at the boundary, namely that

$$R + T = 1 \tag{4.33-1}$$

We consider a stationary frame of reference and another frame of reference moving with velocity $\bar{u}$. Denote quantities expressed in the rest frame by the subscript zero, and those in the moving frame without any subscript. Apply the rules of Galilean transformation to the energy-momentum tensor. It can be shown that the element of the tensor which defines the wave momentum density $\bar{M}$, given by

$$\bar{M} = \frac{U}{\omega} \bar{k} \tag{4.33-2}$$

is an invariant, but that the tensor elements defining the energy density U and energy flux $\bar{F}$ depend on the reference frame.[69,70] Using vector and scalar quantities the following equations hold

$$\bar{M}_o = \bar{M} \tag{4.33-3}$$

$$U_o = U - \bar{u}\cdot\bar{M}_o = \frac{\omega_o}{\omega} U \tag{4.33-4}$$

$$\bar{F}_o = U_o \bar{v}_{go} \tag{4.33-5}$$

$$\bar{v}_{go} = \bar{v}_g + \bar{u} \tag{4.33-6}$$

Here $\omega_o = \omega - \bar{u}\cdot\bar{k}$, and $\bar{v}_g$ is the group velocity of the wave.

Consider two media as described in Section 4.31, and require that in the rest frame of the moving medium in which the incident wave is propagating the incident normal flux equals the sum of the transmitted and reflected normal energy fluxes. Let $\bar{n}$ be a unit vector normal to the boundary and directed into the stationary medium, i.e., from medium (1) to medium (2). Since $\bar{u}$ is parallel to the boundary,

$$v_{go,n} = v_{g,n} \tag{4.33-7}$$

Taking the inner product of the energy flux with $\bar{n}$, yields

$$-\frac{F_{o,nr}}{F_{o,ni}} + \frac{F_{o,nt}}{F_{o,ni}} = 1 \tag{4.33-8}$$

or

$$-\frac{F_{o,nr}}{F_{o,ni}} + \frac{\omega_o}{\omega}\frac{F_{nt}}{F_{o,ni}} = 1 \tag{4.33-9}$$

where equations (4.33-4) and (4.33-7) were used to show that $F_{o,n} = (\omega_o/\omega)F_n$. Substituting for the expression of the normal energy flux

and noting that $\omega_o = \omega_1$, $\omega = \omega_2$ and $k_{nr} = -k_{ni}$, yields

$$\left(\frac{p_r'}{p_i'}\right)^2 + \left(\frac{\omega_2/k_2}{S_2}\right)^4 \left(\frac{\omega_1/k_1}{S_1}\right)^{-4} \left[\frac{\omega_1^2-(\bar{k}_1\cdot\bar{A}_1)^2}{\omega_2^2-(\bar{k}_2\cdot\bar{A}_2)^2}\right]\left(\frac{p_t'}{p_i'}\right)^2 \frac{\rho_{01}k_{nt}}{\rho_{02}k_{ni}} = 1 \quad (4.33\text{-}10)$$

On using the boundary equations (4.31-9) and (4.31-13) together with equations (4.32-4) and (4.32-5), the following identity is obtained

$$\left(\frac{p_r'}{p_i'}\right)^2 + \left(1 + \frac{p_r'}{p_i'}\right)\left(1 - \frac{p_r'}{p_i'}\right) = 1 \quad (4.33\text{-}11)$$

which demonstrates the continuity of normal energy flux across a shear layer.

It can be seen from equation (4.33-4) that, while U_o is by definition positive, the magnitude of U in the frame of reference fixed in medium (2) can take on negative values for sufficiently high values of the streaming velocity $\bar{u}$ and for certain angles of incidence. Thus the wave transmitted across an interface can appear to carry a deficiency of energy with it, as discussed in the previous section. Under these circumstances, the reflected wave will be amplified so that $R > 1$.

4.34 Expression for Snell's Law

We shall restrict ourselves to propagation of nonevanescent plane waves. Furthermore, we chose to define angles of incidence, reflection and refraction as viewed from the rest frame in medium (2). Then the

angles of incidence, reflection and refraction as determined by equation (4.31-16) are related by Snell's law

$$k_\ell = k_1 \sin \alpha_1 = k_2 \sin \alpha_2 \tag{4.34-1}$$

Figure 6 illustrates the geometry at hand. Using equation (4.31-17), equation (4.34-1) can be written as

$$\sin \alpha_2 = \frac{S_2}{S_1} \frac{W_2}{M \cos \xi + W_1} \sin \alpha_1 \tag{4.34-2}$$

in which $W = (\omega/kS)$, $M = (u/S_1)$ is the Mach number and $\cos \xi = (\bar{u}\cdot\bar{k}_1/uk_1)$. Note that in deriving the coefficient of $\sin \alpha_1$ the identity $\omega_2 = \omega_1 + \bar{u}\cdot\bar{k}_1$ is assumed to be a non-zero quantity so as to allow the perturbation frequency to be observed in the rest frame of medium (2). Let

$$Q = \frac{S_1}{S_2} (M \cos \xi + W_1) \tag{4.34-3}$$

and write the dispersion relation in medium (2) as follows

$$W_2 = \pm \left[\frac{1}{2} (1 + q_2^2) \pm \frac{1}{2} \sqrt{(1 + q_2^2)^2 - 4q_2^2 \cos^2 \theta_2} \right]^{\frac{1}{2}} \tag{4.34-4}$$

in which, as before, $q = (A/S)$, and where, from Figure 6,

$$\cos \theta_2 = \sin \alpha_2 \cos \beta_2 \tag{4.34-5}$$

$$\cos \beta_2 = \frac{\bar{k}_\ell \cdot \bar{B}_{02}}{k_\ell B_{02}} \tag{4.34-6}$$

After substituting equations (4.34-4) and (4.34-5) in equation (4.34-2), squaring twice, and collecting terms, the final form for

FIGURE 6.

Geometry of the Incident, Reflected and

Transmitted Waves Across the Plane Boundary

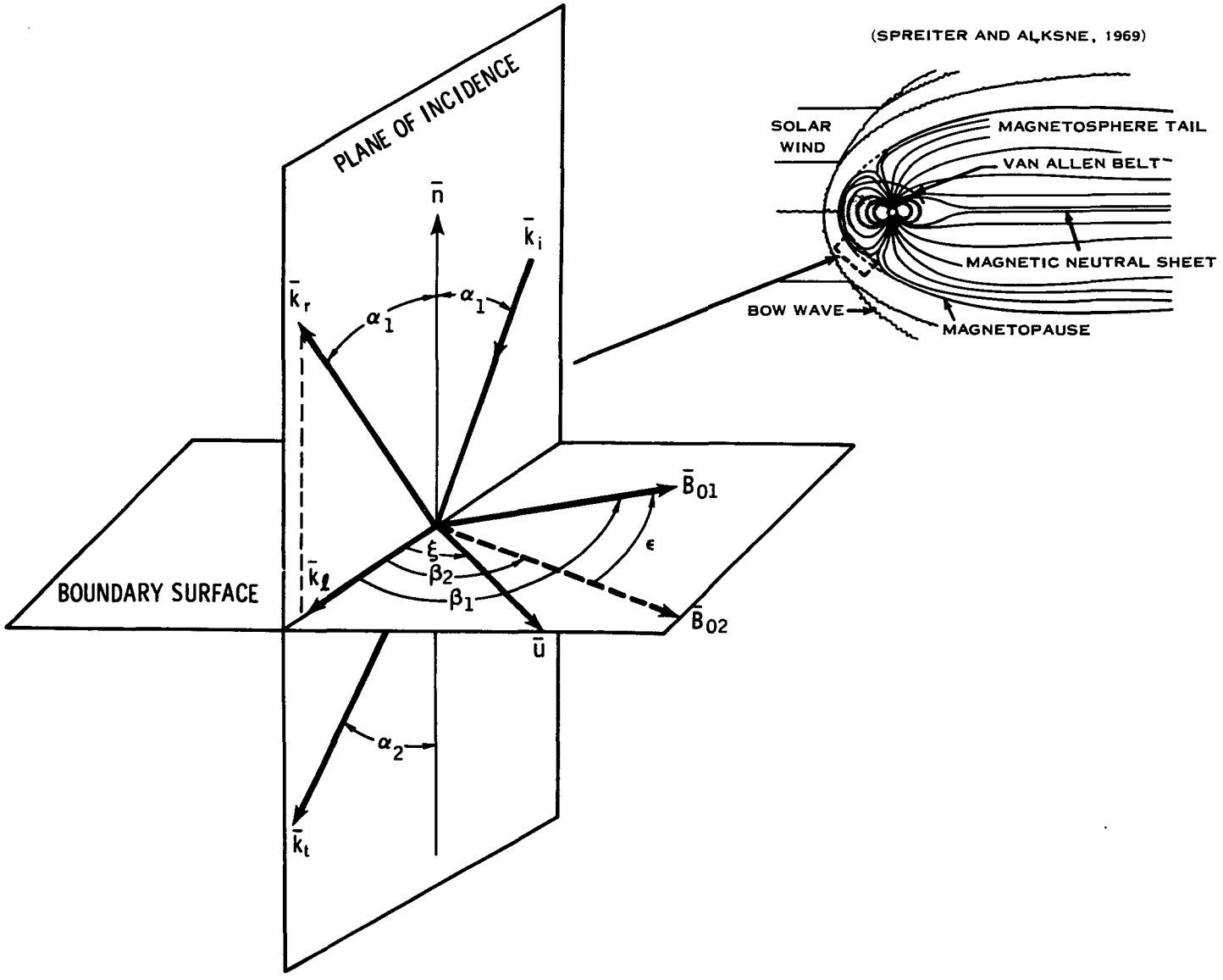
PLANE OF INCIDENCE
BOUNDARY SURFACE
$\bar{n}$
$\bar{k}_i$
$\bar{k}_r$
$\bar{k}_t$
α_1
α_1
α_2
$\bar{B}_{01}$
$\bar{B}_{02}$
ϵ
ξ
β_2
β_1
$\bar{u}$
(SPREITER AND ALKSNE, 1969)
SOLAR WIND
MAGNETOSPHERE TAIL
VAN ALLEN BELT
MAGNETIC NEUTRAL SHEET
BOW WAVE
MAGNETOPAUSE

Snell's law at a fluid velocity discontinuity is obtained, as

$$\sin^2 \alpha_2 = \frac{1}{Q^4}\left[Q^2(1 + q_2^2) - q_2^2 \sin^2 \alpha_1 \cos^2 \beta_2\right] \sin^2 \alpha_1 \quad (4.34\text{-}7)$$

Since the same $\bar{k}_\ell$ is common to the incident and refracted waves, the ambiguity of the sign in the quadratic is resolved by requiring that both incident and refracted angles have the same sign.

4.35 Amplitude and Wavelength of Boundary Oscillations

Let δ_o be the magnitude of the displacement of the boundary surface from the undisturbed position resulting from the incidence of a magnetoacoustic wave. The vanishing of the normal components of magnetic field and velocity requires that equation (4.31-13) be satisfied, that is

$$\frac{1}{\omega_1}(v'_{ni} + v'_{nr}) = \frac{v'_{nt}}{\omega_2} \quad (4.35\text{-}1)$$

which is δ_o. Substituting equations (4.31-5) and (4.32-9) in equation (4.35-1) yields

$$\delta_o = \left(\frac{2}{1+Z}\right)\frac{b'_{ni}}{\bar{k}_1 \cdot \bar{B}_{01}} \quad (4.35\text{-}2)$$

From the requirement that $\bar{b}'$ lie in the plane defined by $\bar{k}$ and $\bar{B}_o$ (see Section 3.20) and from the geometry in Figure 6, it can be shown that

$$b'_n = b' \cos\theta \cos\alpha \quad (4.35\text{-}3)$$

Then

$$\delta_o = \left(\frac{2}{1+Z}\right) \frac{b_i' \cos \alpha_1}{k_1 B_{01}} \tag{4.35-4}$$

is the displacement of the interface due to the perturbation field b'. The wavelength of the ripples induced on the boundary will depend on the magnitude of the tangential component of the incident wave vector, as follows

$$\lambda_\ell = \frac{2\pi}{k_\ell} \tag{4.35-5}$$

For waves normally incident on the boundary, k_ℓ is zero and hence $\lambda_\ell = \infty$. In this case $\omega_2 = \omega_1$ (by equation (4.31-17)) and the displacement of the interface can be calculated from (4.35-1).

4.36 Transfer of Momentum and Energy

Consider the time averaged mangitude of the energy flux density as seen by an observer stationary in medium (2). The general expression for $\langle U' \rangle$ was obtained in Section 3.60, and is repeated here

$$\langle U_2' \rangle = \frac{1}{2} \left[\frac{\omega_2^2 - k_2^2 S_2^2 (\bar{k}_2 \cdot \bar{A}_2)^2}{\omega_2^2 - (\bar{k}_2 \cdot \bar{A}_2)^2} \right] \frac{\rho_t'}{\rho_{02} k_2^2}$$

$$= \frac{1}{2} \left(\frac{W_2^4 - q_2^2 \cos^2 \theta_2}{W_2^2 - q_2^2 \cos^2 \theta_2} \right) \frac{p_t'^2}{S_2^2 \rho_{02}} \tag{4.36-1}$$

where $W = (\omega/kS)$, $q = (A/S)$, and where the relation $p' = S^2 \rho'$ was used. The pressure balance of the perturbation stresses can be written as

$$p_t' = \left(\frac{W_1}{W_2}\right)^2 \left(1 + \frac{p_r'}{p_i'}\right) p_i' \tag{4.36-2}$$

Furthermore, from equation (4.31-8)

$$p_i' = \frac{\bar{B}_{01} \cdot \bar{b}_i'}{4\pi\mu(W_1^2 - 1)}$$

$$= \frac{B_{01}\, b_i' \sin\theta_1}{4\pi\mu(W_1^2 - 1)} \tag{4.36-3}$$

Substituting equations (4.36-2) and (4.36-3) in equation (4.36-1) yields

$$\langle U_2' \rangle = \frac{1}{2}\left(\frac{1}{4\pi\mu}\right)^2 \left(\frac{W_1}{W_2}\right)^4 \left(\frac{W_2^4 - q_2^2 \cos^2\theta_2}{W_2^2 - q_2^2 \cos^2\theta_2}\right) \left(\frac{B_{01} b_i' \sin\theta_1}{W_1^2 - 1}\right)^2 \left(1 + \frac{p_r'}{p_i}\right)^2 \frac{1}{S_2^2 \rho_{02}}$$

$$= \frac{q_1^2}{8\pi\mu} \left(\frac{\gamma^{-1} + \frac{1}{2} q_2^2}{\gamma^{-1} + \frac{1}{2} q_1^2}\right) \left(\frac{W_1}{W_2}\right)^4 \left(\frac{W_2^4 - q_2^2 \cos^2\theta_2}{W_2^2 - q_2^2 \cos^2\theta_2}\right) \left(\frac{1 + p_r'/p_i'}{W_1^2 - 1}\right)^2 b_i'^2 \sin^2\theta_1 \tag{4.36-4}$$

in which use of equation (4.31-2) was made to obtain the last step.

Finally, the time averaged momentum density is simply given by

$$\langle \bar{M}_2' \rangle = \frac{\langle U_2' \rangle}{S_2 W_2} \frac{\bar{k}}{k} \tag{4.36-5}$$

4.40 Calculations and Discussion

Before proceeding with the actual calculations, the allowed range of phase velocities for MHD waves in a perfectly conducting fluid permeated by a homogeneous magnetic field B is considered. In Figure 7 the roots of the dispersion relation (equation (4.34-4)) are plotted against the Alfvén velocity in units of sound velocity. The shaded portions of the dimensionless plot denote regions where propagation of MHD waves is allowed. The boundaries of these regions correspond to $\theta = 0$ and $\theta = \pi/2$, where $\cos\theta = \bar{B}_o \cdot \bar{k}/B_o k$. In the upper narrow band waves propagate in the fast mode, while in the lower band they propagate in the slow mode. For given properties of the medium which specify the parameter q, it can be seen that waves propagating in the slow mode have a considerably larger range of allowed phase velocities than those propagating in the fast mode. The latter waves approach the Alfvén velocity for large values of q, such as are found in the inner magnetosphere. For normal solar wind conditions at the Earth's orbit one expects $q < 1$, while in the sunward magnetosheath q should be of order unity. However, since the magnetosheath is a turbulent transition-region, one can anticipate a considerable spread in q-values.

Recently, Ogilvie et al.,[65] have reported on observations in the magnetosheath near the dawn magnetopause during magnetically quiet as well as disturbed conditions. At the bottom of Figure 7 several values of q derived from these observations are indicated where the ratio of specific heats γ is taken to be 5/3 in evaluating q. The two highest q values in the range correspond to magnetically quiet conditions. The

FIGURE 7.

Plot of the Ratio of Phase Velocity to Sound Velocity $(\frac{\omega/k}{S})$ Against the Ratio of Alfvén to Sound Velocity $q = (A/S)$. Also Shown are Examples of Measured Magnetosheath Values for q

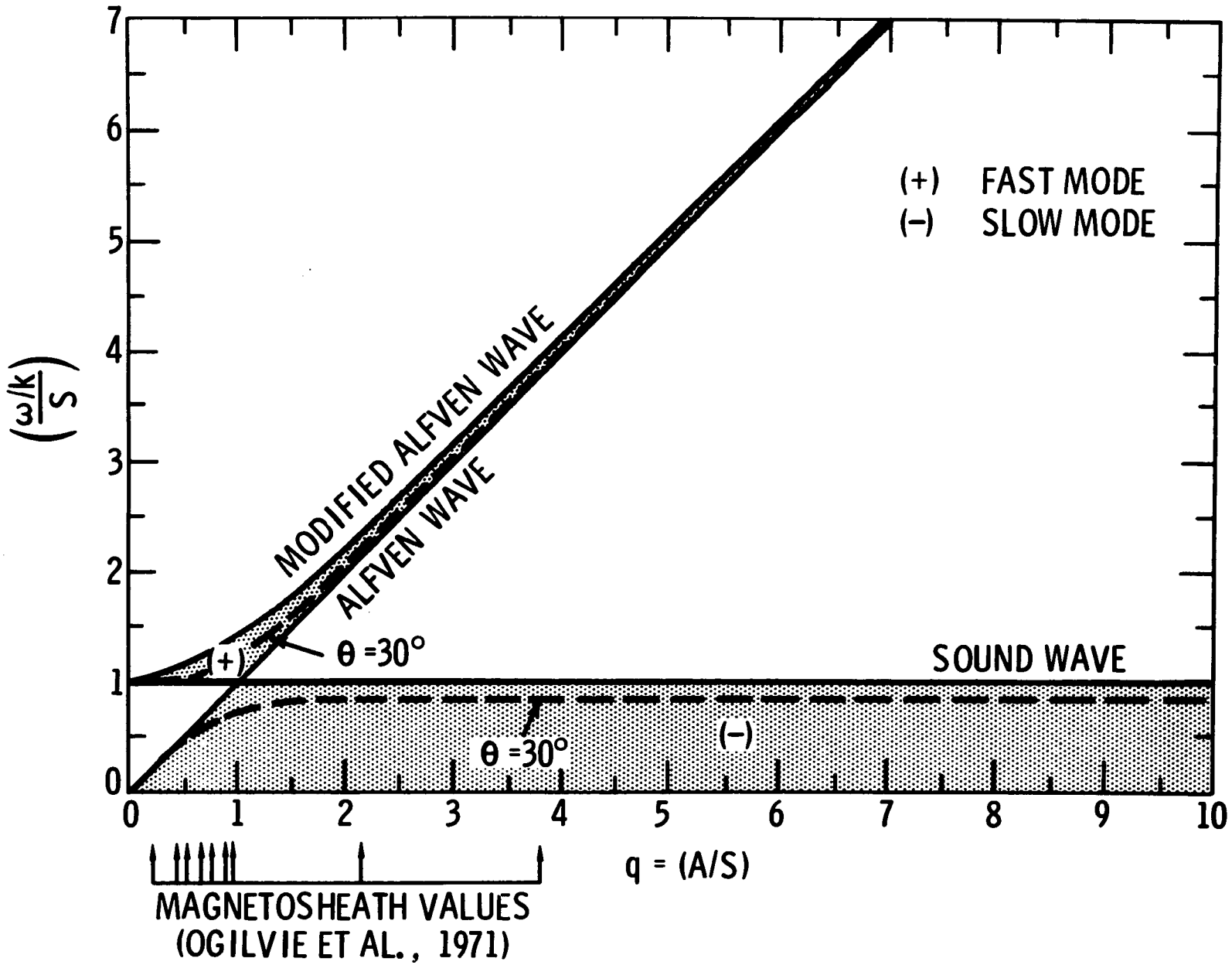
7
6
5
4
3
2
1
0
$\left(\frac{\omega/k}{S}\right)$
(+) FAST MODE
(−) SLOW MODE
MODIFIED ALFVEN WAVE
ALFVEN WAVE
θ =30°
(+)
SOUND WAVE
θ =30°
(−)
0 1 2 3 4 5 6 7 8 9 10
q = (A/S)
MAGNETOSHEATH VALUES
(OGILVIE ET AL., 1971)

variability of conditions in the magnetosheath is evident from the spread shown.

In the following analysis the response of the magnetopause to MHD waves impinging on its surface is discussed. These waves are taken to originate in the magnetosheath with an isotropic flux distribution. The calculations are restricted to those parameters of the magnetopause which correspond to the sunward portion of the boundary during quiet conditions of the solar wind. The pressure balance across the magnetopause yields

$$\frac{B_m^2}{8\pi} + N_m k T_m = \frac{B_s^2}{8\pi} + N_s k T_s (1+X) \qquad (4.40\text{-}1)$$

Here the subscripts m and s refer to quantities pertinent to the magnetosphere and magnetosheath respectively, and T is the temperature of the plasma. The factor $X = (\rho u^2 / N_s k T_s)$ accounts for the solar wind dynamic pressure on the magnetosheath side of the boundary. Listed in Table 2 are two sets of parameters which satisfy the pressure balance relation and which will be discussed in this section. Case 1 is taken as representative of magnetopause conditions in the vicinity of the subsolar point; Case 2 as representative of magnetopause conditions near the dusk and/or dawn meridian. In the analysis to follow it is assumed for simplicity that the magnetosheath field $\bar{B}_s$ is uniform and steady and lies in the plane of the magnetopause. It is also assumed that the streaming velocity vector $\bar{u}$ of the solar wind plasma is parallel to $\bar{B}_s$. The result would be the same if any velocity vector perpendicular to $\bar{B}_s$ is added to this $\bar{u}$ so long as the added vector is parallel to the

TABLE 2

Pressure Balance Parameters for the Sunward Magnetopause

Case	N_{sphere} (cm^{-3})	N_{sheath} (cm^{-3})	B_{sphere} (gamma)	B_{sheath} (gamma)	T_{sphere} (10^5°K)	$T_{sheath}(1+X)$ (10^5°K)
1	1	31.5	50	10	2.0	22.0
2	1	20.9	30	20	2.0	7.0

boundary surface. Referring to Figure 6, the following quantities are defined:

$$\begin{aligned} B_{01} &\equiv B_s \\ B_{02} &\equiv B_m \\ \xi &= \beta_1 \\ \epsilon &= \cos^{-1}\left[\bar{B}_s \cdot \bar{B}_m / B_s B_m\right] \end{aligned} \tag{4.40-2}$$

Figures 8 and 9 show plots of the transmission coefficient T against the angle of incidence α_1 for selected values of the azimuthal angle β_1. A convention is adopted so that α_1 is positive for waves whose propagation vector $\bar{k}$ has a component along the flow vector $\bar{u}$. The angles β_1 and β_2 defined in each medium by $\cos \beta = \bar{k}_\ell \cdot \bar{B}_o / k_\ell B_o$, are measured positively counter-clockwise. Figure 8 refers to Case 1 and illustrates the conditions $\epsilon = 0°$ and $90°$ for the indicated values of the flow Mach number. Figure 9 is a similar plot referring to Case 2. It can be seen that in the frame of reference of medium (2), appreciable transmission into the magnetosphere occurs only for incoming fast waves which propagate over a small range of angles near the normal incidence. It is noted that transmission occurs over a wider range of angles for positive α_1 than for negative α_1. The degree of this asymmetry increases with increasing Mach number. As expected, the asymmetry disappears for waves having planes of incidence normal to the streaming vector (i.e. $\beta_1 = 90°$). Also shown in Figures 8 and 9 are maximum and minimum values of α_1^* which is the incident angle in a frame of reference fixed in the streaming plasma. The incident angles in the inertial and

FIGURE 8.

Plot of the Transmission Coefficient T Against the Angle of Incidence α_1 for Case 1

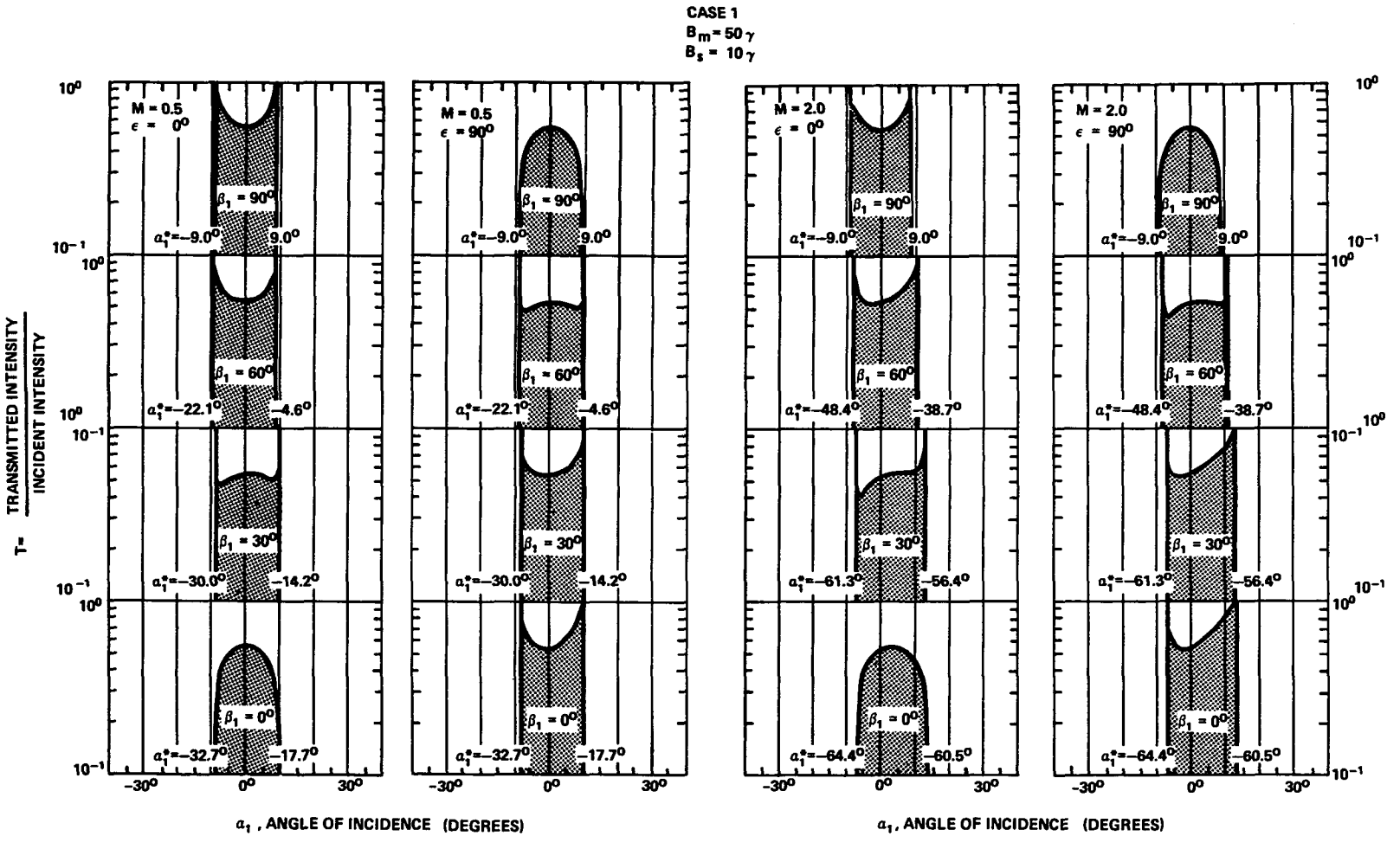
CASE 1
$B_m = 50\gamma$
$B_s = 10\gamma$
M = 0.5
ϵ = 0°
M = 0.5
ϵ = 90°
M = 2.0
ϵ = 0°
M = 2.0
ϵ = 90°
β_1 = 90°
β_1 = 60°
β_1 = 30°
β_1 = 0°
α_1^*=−9.0°
9.0°
α_1^*=−22.1°
−4.6°
α_1^*=−30.0°
−14.2°
α_1^*=−32.7°
−17.7°
α_1^*=−48.4°
−38.7°
α_1^*=−61.3°
−56.4°
α_1^*=−64.4°
−60.5°
10^0
10^{-1}
−30°
0°
30°
T= TRANSMITTED INTENSITY / INCIDENT INTENSITY
α_1, ANGLE OF INCIDENCE (DEGREES)
α_1, ANGLE OF INCIDENCE (DEGREES)

FIGURE 9.

Plot of the Transmission Coefficient T Against

the Angle of Incidence α_1 for Case 2

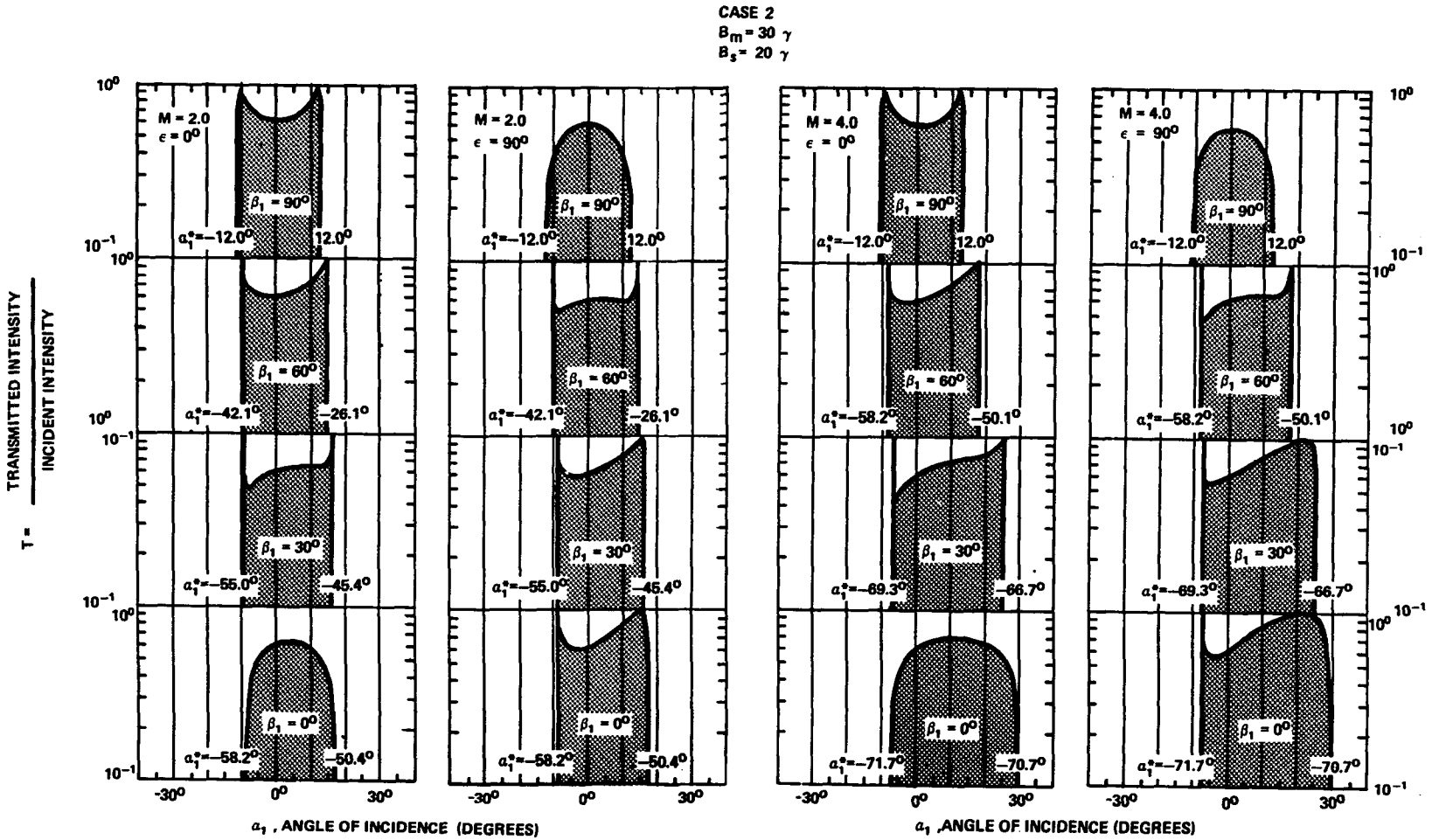
CASE 2
B_m = 30 γ
B_s = 20 γ
T = TRANSMITTED INTENSITY / INCIDENT INTENSITY
M = 2.0
ε = 0°
M = 2.0
ε = 90°
M = 4.0
ε = 0°
M = 4.0
ε = 90°
β1 = 90°
α1*=−12.0°
12.0°
β1 = 60°
α1*=−42.1°
−26.1°
α1*=−58.2°
−50.1°
β1 = 30°
α1*=−55.0°
−45.4°
α1*=−69.3°
−66.7°
β1 = 0°
α1*=−58.2°
−50.4°
α1*=−71.7°
−70.7°
10⁰
10⁻¹
-30°
0°
30°
α1 , ANGLE OF INCIDENCE (DEGREES)

moving frames are related by

$$\tan \alpha_1^* = \frac{W_1 \sin \alpha_1 - M \cos \xi}{W_1 \cos \alpha_1} \qquad (4.40\text{-}3)$$

The values of α_1^* shown in Figures 8 and 9 indicate that most transmission occurs for waves propagating upstream.

The asymmetric behavior is further illustrated in Figures 10 and 11 for Cases 1 and 2 respectively as seen from the magnetosphere. Each figure shows polar plots of both reflection and transmission coefficients and their corresponding angles of incidence and refraction, for $\beta_1 = 0^\circ$ and $\varepsilon = 90^\circ$. The interface separating the magnetosphere from the magnetosheath region corresponds to $\alpha_1 = \pm 90^\circ$. The unshaded area in the upper portion of each plot denotes the window for which partial reflection occurs. The transmission coefficients for these transmitted waves are shown by the shaded area in the lower portion of the same plot. As before, incidence angles of waves having k_ℓ along the flow vector $\bar{u}$ are shown as positive. The arrows in the diagram on the left hand side of Figures 10 and 11 show a representative correspondence between reflected and transmitted waves. It can be seen from the figures that the transmitted wave is refracted at angles larger than the corresponding incidence angles. It is noted that in both Figures 10 and 11 there is a remarkable difference in the shape of the distribution of the transmission coefficient between the two angles of ε considered, i.e. $\varepsilon = 0^\circ$ and $\varepsilon = 90^\circ$. For the case when the magnetic fields in the two media are perpendicular to each other ($\varepsilon = 90^\circ$), more energy flux is transmitted at large angles of refraction than at small angles of refraction. The excess in energy flux

FIGURE 10.

Polar Plot of the Reflection and Transmission Coefficients R and T for Case 1 and for $\beta_1 = 0°$, $\varepsilon = 0°, 90°$

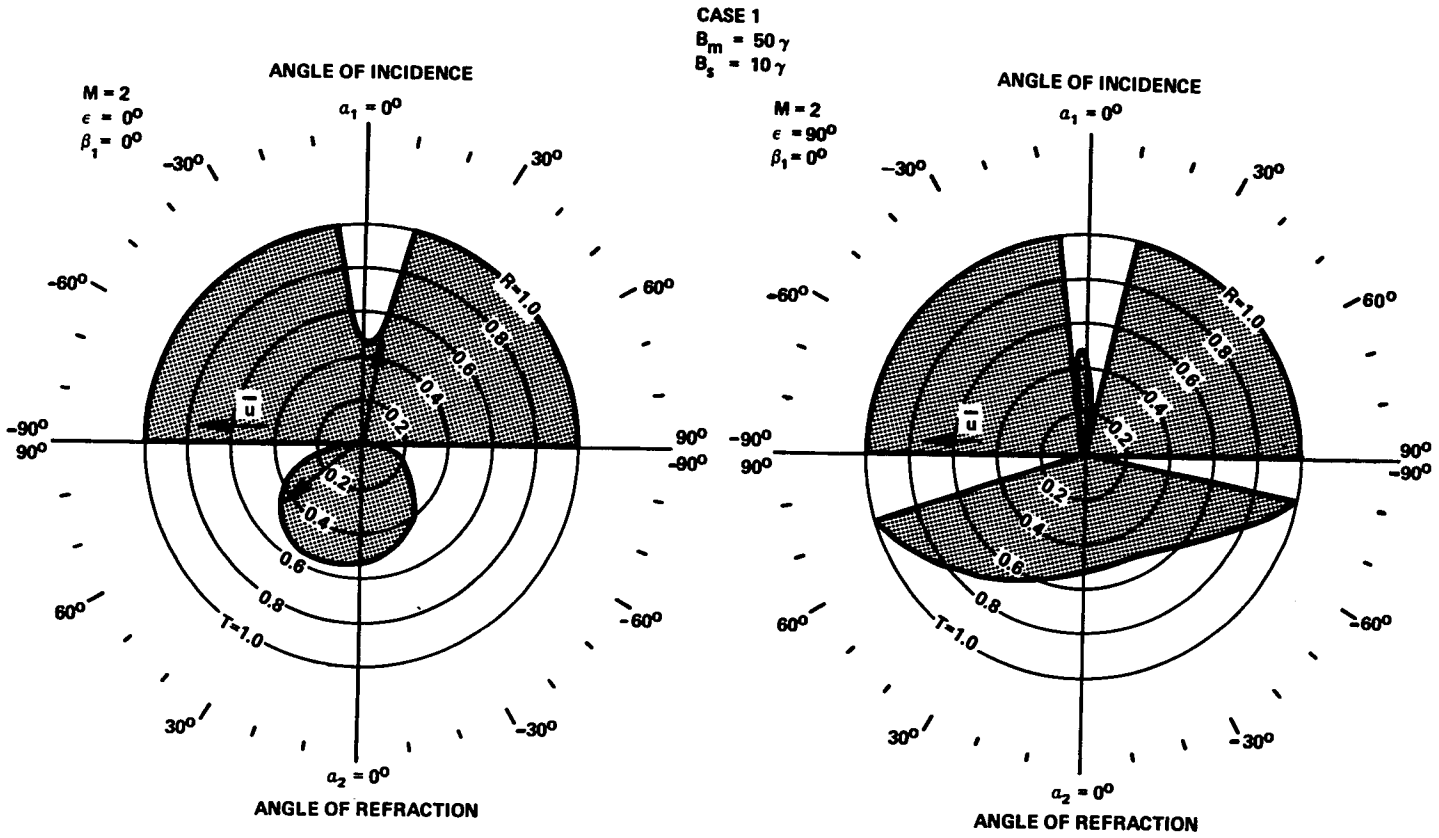
CASE 1
B_m = 50 γ
B_s = 10 γ
M = 2
ϵ = 0°
β_1 = 0°
ANGLE OF INCIDENCE
α_1 = 0°
-30°
30°
-60°
60°
-90°
90°
R=1.0
0.8
0.6
0.4
0.2
I=1
0.2
0.4
0.6
0.8
T=1.0
α_2 = 0°
ANGLE OF REFRACTION
M = 2
ϵ = 90°
β_1 = 0°
ANGLE OF INCIDENCE
α_1 = 0°
ANGLE OF REFRACTION
α_2 = 0°

FIGURE 11.

Polar Plot of the Reflection and Transmission Coefficients R and T for Case 2 and for $\beta_1 = 0°$, $\varepsilon = 0°, 90°$

CASE 2
Bm = 30 γ
Bs = 20 γ

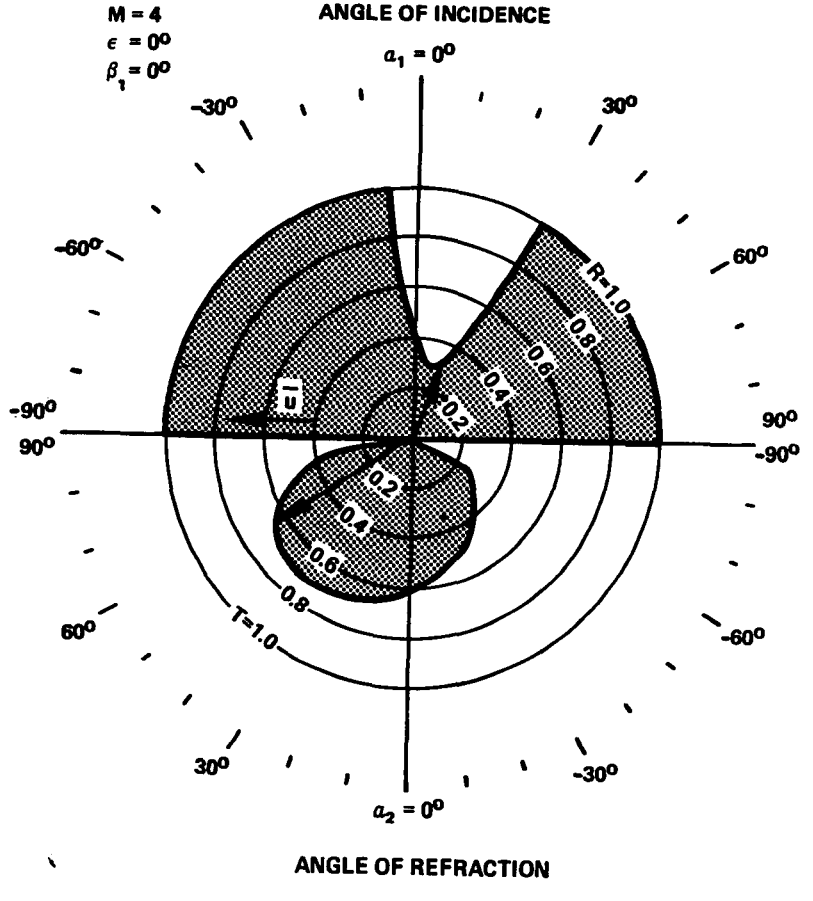

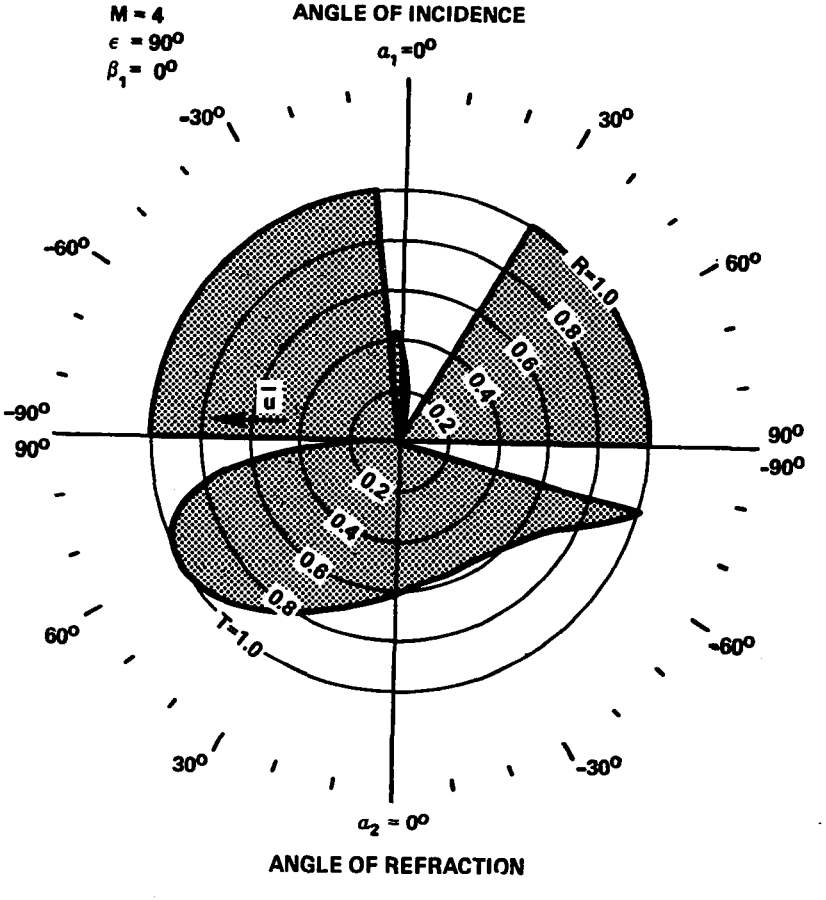

transmitted by waves with $\alpha_2 > 0$ over waves with $\alpha_2 < 0$, represents the drag energy associated with the MHD waves.

The total energy density and momentum of the transmitted waves can be evaluated by integrating equations (4.36-4) and (4.36-5) over all angles of the incident flux. For simplicity this flux is assumed to be isotropic relative to the magnetosphere. The results of such a calculation are shown in Table 3, together with the integrated values of the reflection and transmission coefficients. For the chosen magnetopause parameters, only about 1 to 2 percent of the incident energy flux is transmitted into the magnetosphere. Thus, during quiet conditions of the solar wind the sunward magnetosphere may indeed seem to behave like a near perfect reflector to the MHD waves as was summised by McKenzie.[51] Yet, when integrating the flux transmitted into the magnetosphere from waves having an amplitude of say 1 gamma, it is found that roughly 10^{-6} to 10^{-5} erg cm^{-2} sec^{-1} are being deposited in the sunward magnetosphere. Assuming a steady isotropic flux incident on a hemispherical magnetopause of radius 15 R_E, the total energy input into the magnetosphere is estimated to be of the order 10^{21} erg per day. This energy amounts to about ten percent of the total energy in the range 20 ev $\leq E \leq$ 50 kev for trapped particles residing between $1 \leq L \leq 8$ ($\sim 10^{22}$ erg)[73], and therefore it is likely to contribute significantly to the energy budget of the magnetosphere.

Measurements show that the energy density of the turbulent wave spectrum in the sunward magnetosheath is $\varepsilon \simeq 10^{-9} - 10^{-10}$ erg/cm^3.[40,41,74,75] The momentum density of the waves can be estimated to be

TABLE 3

Values of Transmitted and Reflected Quantities
for $\varepsilon = 0°$ and $\varepsilon = 90°$

ε	Case	Propagation Mode	Mach No.	R	T	Transmitted Momentum ($\times 10^{-21}$ erg-sec-cm^{-4}-gamma^{-2})	Transmitted Energy ($\times 10^{-13}$ erg-cm^{-3}-gamma^{-2})
0°	1	Fast	0.5-2	0.99	1×10^{-2}	2.6	2.8
		Slow		1.0	0	0	0
	2	Fast	2-4	0.98	2×10^{-2}	0.9-3.5	0.6-2.3
		Slow		1.0	0	0	0
90°	1	Fast	0.5-2	0.99	1×10^{-2}	3.0	3.2
		Slow		1.0	0	0	0
	2	Fast	2-4	0.98	2×10^{-2}	1.1-4.0	0.7-2.6
		Slow		1.0	0	0	0

$$M \simeq \varepsilon/(\omega/k) \simeq 10^{-16} - 10^{-17}\ g/cm^2\text{-}cm \qquad (4.40\text{-}4)$$

for phase velocities of the order 10^2 km/sec, which is taken to be typical for this region of space. Thus the transmitted energy density and momentum calculated in Table 3 represent approximately a fraction to a few percent of the energy and momentum density available in the wave spectrum of the magnetosheath during quiet conditions. The problem of how the wave energy transmitted into the magnetosphere interacts with the plasma is complex and is beyond the scope of the present work.

Finally consider the amplitude and wavelength of the oscillation of the boundary surface (equations (4.35-4) and (4.35-5)). In Figure 12, ranges in wavelength against frequency of the incident perturbation are plotted for the Mach numbers of plasma flow shown. Since the hydromagnetic frequency domain lies well below the gyrofrequency of ions, values of proton gyrofrequencies in ambient fields of 10, 30 and 60 gamma are also given in the figure. Case 2 exhibits a slightly larger range in wavelengths than Case 1, and the dependence of both cases on the Mach number is small. The curves are labeled with critical values of α_1 for which boundary ripples can be set up.

Measurements of MHD perturbations in the magnetosheath indicate a maximum power density in the range 10^{-3} - 10^{-2} hertz.[40,41,74,75] Wavelengths of the boundary oscillations for these frequencies are comparable to the sunward dimensions of the magnetosphere. Therefore, for these frequencies the plane wave treatment considered above does not apply. For the theory to be valid the frequency of the incident MHD waves must be less than about 10^{-1} hertz for plasma conditions of

FIGURE 12.

Ranges for Wavelength of the Boundary Oscillations

as a Function of Frequency of the Incident MHD Waves,

for Cases 1 and 2

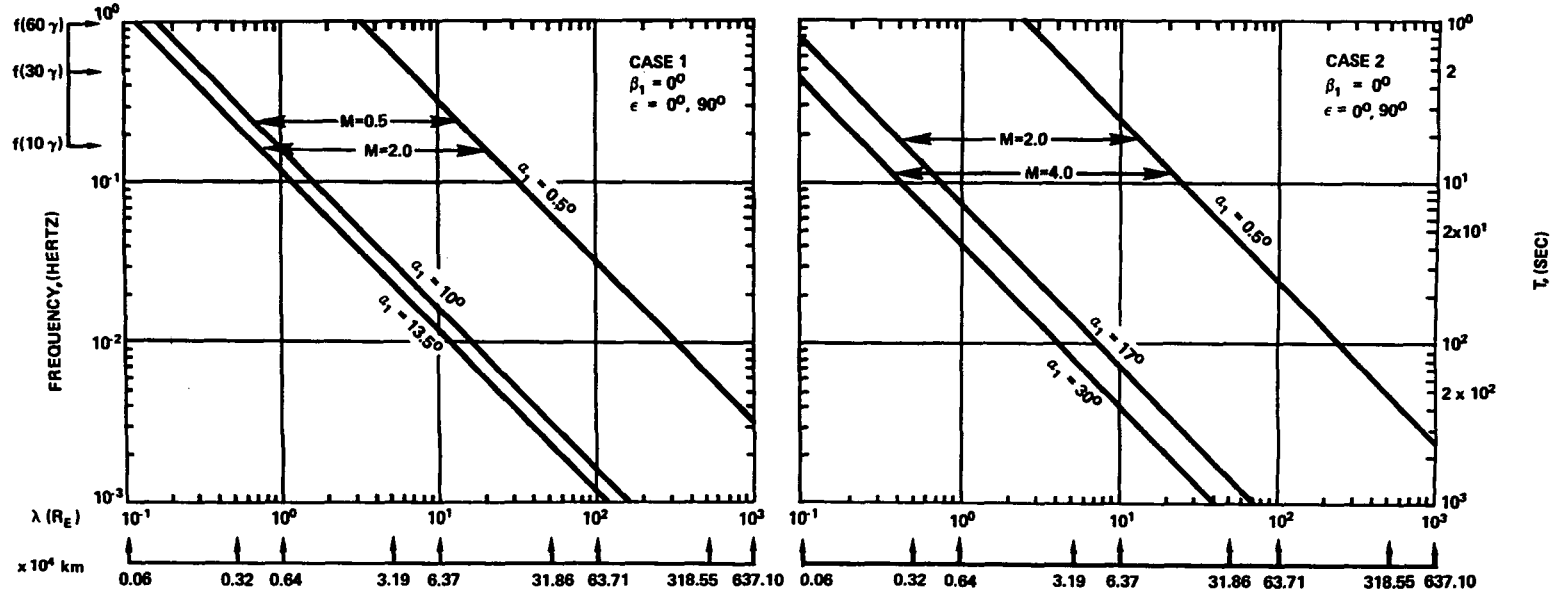
f(60 γ)
f(30 γ)
f(10 γ)
FREQUENCY, (HERTZ)
λ (R_E)
x 10^4 km
CASE 1
β1 = 0°
ε = 0°, 90°
M=0.5
M=2.0
α1 = 0.5°
α1 = 10°
α1 = 13.5°
CASE 2
β1 = 0°
ε = 0°, 90°
M=2.0
M=4.0
α1 = 0.5°
α1 = 17°
α1 = 30°
τ, (SEC)
0.06
0.32
0.64
3.19
6.37
31.86
63.71
318.55
637.10

the kind dealt with here. Even for a frequency near 10^{-1} hertz, the wavelength can be comparable with the dimensions of the magnetosphere for waves arriving near normal incidence.

In Figure 13, the range of amplitudes of the magnetopause ripples per gamma of incident perturbation, is plotted against the incomming MHD frequencies. As was the case for λ in the previous figure, the dependence of the amplitudes on Mach number is negligible. For waves with frequency of 10^{-1} hertz the amplitude of the boundary oscillation is less than 5×10^{-3} R_E per gamma of incident wave amplitude. Motion of the magnetopause with amplitude of approximately 1 R_E have been previously noted by many authors.[53,65,76] These oscillations have much lower frequencies than the lowest frequency to which the present theory can be applied. Since a boundary crossing takes typically a minute, it is impossible to detect oscillations of the boundary with a frequency of 10^{-1} hertz.

FIGURE 13.

Range of Amplitudes of the Boundary Oscillations as a Function of Frequency of the Incident MHD Waves, for Cases 1 and 2

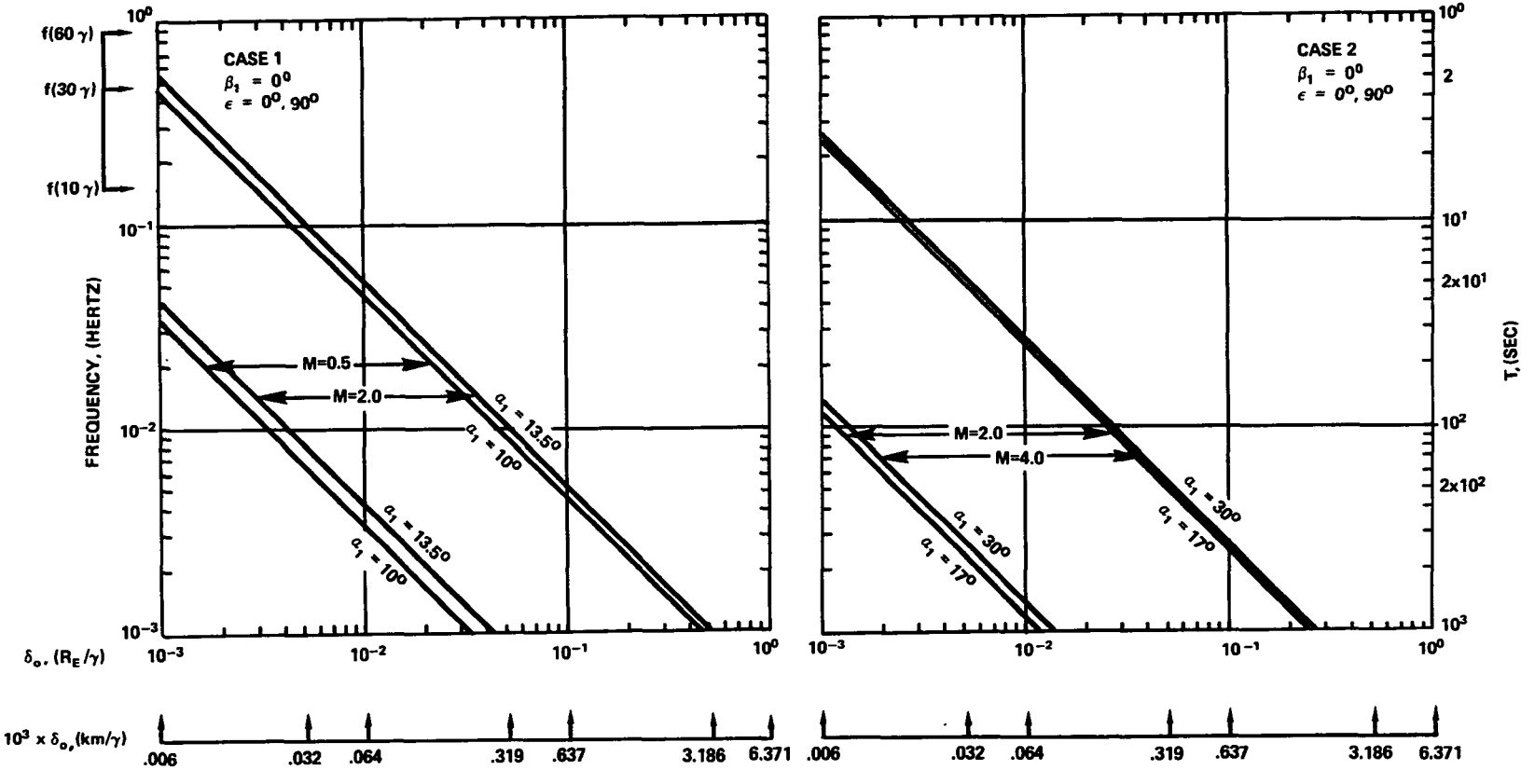
f(60 γ)
f(30 γ)
f(10 γ)
CASE 1
$\beta_1 = 0^0$
$\epsilon = 0^0, 90^0$
M=0.5
M=2.0
$\alpha_1 = 13.5^0$
$\alpha_1 = 10^0$
$\alpha_1 = 13.5^0$
$\alpha_1 = 10^0$
FREQUENCY, (HERTZ)
10^0
10^{-1}
10^{-2}
10^{-3}
δ_o, (R_E/γ)
10^{-3}
10^{-2}
10^{-1}
10^0
$10^3 \times \delta_o$, (km/γ)
.006
.032
.064
.319
.637
3.186
6.371
CASE 2
$\beta_1 = 0^0$
$\epsilon = 0^0, 90^0$
M=2.0
M=4.0
$\alpha_1 = 30^0$
$\alpha_1 = 17^0$
$\alpha_1 = 30^0$
$\alpha_1 = 17^0$
10^0
2
10^1
$2x10^1$
10^2
$2x10^2$
10^3
T, (SEC)
10^{-3}
10^{-2}
10^{-1}
10^0
.006
.032
.064
.319
.637
3.186
6.371

5.0 SUMMARY AND CONCLUSIONS

In Chapter 2.0 solar wind data from the Vela 2A satellite are compared with D_{st} values on magnetically quiet days. It is found that the square root of the solar wind pressure is statistically linearly correlated to the hourly D_{st} values. This relation is in accordance with the theoretical expectation from the pressure balance at the magnetopause between the solar wind plasma and the Earth's magnetic field. The constant of proportionality relating daily solar wind pressure changes to the corresponding magnetic field changes at the Earth's surface, shows considerable variation over the time span (July 1964 to July 1965) for which solar wind data were analyzed. The peak in the frequency distribution for this constant is in rough agreement with that obtained by Siscoe et al.[17] and Ogilvie et al.,[19] using a different technique. The average value for the proportionality constant approximately agrees with the theoretical value given by the Mead-Beard[13] magnetosphere model.

Chapter 3.0 is devoted to a general review of magnetohydrodynamic theory. In this chapter the basic MHD equations are developed in a form suitable to their use in the last chapter, where they are applied to the reflection and refraction of hydromagnetic waves at the magnetopause boundary.

In Chapter 4.0 expressions for the reflection and transmission coefficients are calculated for a stable velocity-discontinuity surface separating two compressible, perfectly conducting fluids, each permeated

by a homogeneous magnetic field. The system is perturbed by small amplitude waves in the hydromagnetic frequency range. Reflection and transmission coefficients are evaluated for two cases shown in Table 2 which are taken as being representative of the sunward magnetopause during normal conditions of the solar wind. Numerical values for the coefficients are obtained under the assumption that the streaming velocity vector $\bar{u}$ of the solar wind plasma is parallel to the magnetosheath field $\bar{B}_s$. For the two cases considered it is found that:

(i) Appreciable transmission into the magnetosphere occurs only for incoming fast waves which propagate over a small range of angles near normal incidence.

(ii) Transmission occurs over a wider range of incident angles for waves having a positive component of the propagation vector $\bar{k}$ along the direction of the plasma flow than for waves having a negative component in this direction. This asymmetry increases with increasing Mach number.

(iii) Transmitted waves are refracted at angles larger than the incidence angles.

(iv) When the transmission coefficient is integrated over all angles of an isotropic incident MHD flux, the energy transmitted is only about 1 to 2 percent of the incident flux energy.

The integrated energy density of the waves transmitted into the magnetosphere for the cases under consideration represents a fraction of a

percent to a few percent of the measured energy density in the wave spectrum of the magnetosheath under normal conditions. The energy flux transmitted into the magnetosphere from waves having an amplitude of 1 gamma is roughly of the order 10^{-6} to 10^{-5} erg cm^{-2} sec^{-1}. Assuming a steady isotropic flux of waves with amplitude of 1 gamma incident on a hemispherical sunward magnetospheric boundary of radius 15 R_E, the total energy input into the magnetosphere is estimated to be of the order of 10^{21} erg per day. Transfer of energy and momentum increases with increasing Mach number of the magnetosheath plasma flow.

The incident hydromagnetic waves will cause ripples in the boundary surface. The wavelengths of the boundary ripples for MHD waves having power spectral densities similar to those observed in the magnetosheath range from a few tenths of one earth radius to several hundred R_E. However, the present theory is valid only for wavelengths which are small compared to the dimensions of the magnetosphere.

Discussions presented in this thesis do not purport to be a complete treatment of the processes taking place at the magnetospheric boundary during magnetically quiet conditions. Nevertheless, the results obtained should be indicative of the MHD effects which are likely to occur at the magnetopause, and suggest that transmission of MHD waves across the magnetopause plays an important role in the energy budget of the magnetosphere.

6.0 REFERENCES

[1]C. P. Sonett, D. S. Colburn, L. Davis, E. J. Smith, and P. J. Coleman, Phys. Rev. Letters 13, 153, (1964).

[2]N. F. Ness, J. Geophys. Res. 70, 2989, (1965).

[3]N. F. Ness, K. W. Behannon, S. C. Cantarano, and C. S. Scearce, J. Geophys. Res. 72, 927, (1967).

[4]K. W. Behannon, J. Geophys. Res. 73, 907, (1968).

[5]J. D. Mihalov, D. S. Colburn, R. G. Currie, and C. P. Sonett, J. Geophys. Res. 73, 943, (1968).

[6]D. H. Fairfield and N. F. Ness, J. Geophys. Res. 72, 2379, (1967).

[7]D. H. Fairfield, J. Geophys. Res. 76, 6700, (1971).

[8]W. I. Axford, J. Geophys. Res. 67, 3791, (1962).

[9]P. J. Kellogg, J. Geophys. Res. 67, 3805, (1962).

[10]J. R. Spreiter, A. L. Summers, and A. Y. Alksne, Planet. Space Sci. 14, 223, (1966).

[11]M. Dryer and R. Faye-Petersen, AIAA Journal 4, 246, (1966).

[12]J. E. Midgley and L. Davis, Jr., J. Geophys. Res. 68, 5111, (1963).

[13]G. D. Mead and D. B. Beard, J. Geophys. Res. 69, 1169, (1964).

[14]W. P. Olson, J. Geophys. Res. 74, 1275, (1969).

[15]L. D. Landau and E. M. Lifshitz, Fluid Mechanics (Addison-Wesley Publishing Co., Reading, Mass., 1959).

[16]G. D. Mead, J. Geophys. Res. 69, 1181, (1964).

[17]G. L. Siscoe, V. Formisano, and A. J. Lazarus, J. Geophys. Res. 73, 4869, (1968).

[18]D. B. Beard, J. Geophys. Res. 65, 3559, (1960).

[19]K. W. Ogilvie, L. F. Burlaga, and T. D. Wilkerson, J. Geophys. Res. 73, 6809, (1968).

[20]P. Verzariu, I. B. Strong, and M. Sugiura, Trans. Amer. Geophys. Union 50, 279, (1969).

[21]M. Sugiura, Annals of the International Geophysical Year (Pergamon Press, Oxford, 1964), Vol. 35, p. 9.

[22]M. Sugiura and S. J. Cain, NASA Report No. X-612-69-20, 1969.

[23]S. I. Akasofu, J. C. Cain, and S. Chapman, J. Geophys. Res. 67, 2645, (1962).

[24]R. A. Hoffman and P. A. Bracken, J. Geophys. Res. 72, 6039, (1967).

[25]M. Sugiura, B. G. Ledley, T. L. Skillman, and J. P. Heppner, J. Geophys. Res. 76, 7552, (1971).

[26]M. A. Schield, J. Geophys. Res. 74, 1275, (1969).

[27]L. Lees, AIAA J. 2, 1576, (1964).

[28]N. Herlofson, Nature 165, 1020, (1950).

[29]H. Alfvén, Cosmical Electrodynamics (Clarendon Press, Oxford, 1950).

[30]T. G. Cowling, Magnetohydrodynamics (Interscience Publishers, New York, 1957).

[31]J. Bazer and O. W. Fleischman, Phys. Fluids 2, 366, (1959).

[32]M. J. Lighthill, Phil. Trans., Roy. Soc. (London) A252, 397, (1960).

[33]J. E. Anderson, Magnetohydrodynamic Shock Waves (MIT Press Publishing Co., Cambridge, Mass., 1963).

[34]H. E. Petschek, in AAS-NASA Symposium on the Physics of Solar Flares, Washington, D.C., 1964, edited by W. N. Hess.

[35]T. W. Dungey, Imperial College of Science and Technology, Univ. of London, Report No. SP/67/4, (1967).

[36]W. A. Newcomb, Dynamics of Fluids and Plasmas (Academic Press Inc., New York, 1966).

[37]R. Faye-Petersen and G. Heckman, Ann. Geophys. 24, 347, (1968).

[38]A. Eviatar and R. A. Wolf, J. Geophys. Res. 73, 5561, (1968).

[39]W. I. Axford, Planet. Space Sci. 12, 45, (1964).

[40]R. L. Kaufmann, J. T. Horng, and A. Wolfve, J. Geophys. Res. 75, 4666, (1970).

[41]F. Mariani, B. Bavassano, and N. F. Ness, J. Geophys. Res. 75, 6037, (1970).

[42]J. T. Stuart, Proc. Roy. Soc. A221, 189, (1954).

[43]R. C. Lock, Proc. Roy. Soc. A233, 105, (1955).

[44]W. I. Axford, Q. J. Mech. Appl. Math. 13, 314, (1960).

[45]W. I. Axford, Can. J. Phys. 40, 654, (1962).

[46]S. Chandrasekhar, Hydrodynamic and Hydromagnetic Stability (Oxford University Press, London, 1961).

[47]J. A. Fejer, Physics Fluids 7, 499, (1964).

[48]A. K. Sen, Planet. Space Sci. 13, 131, (1965).

[49]I. Lerche, J. Geophys. Res. 71, 2365, (1966).

[50]D. J. Southwood, Planet. Space Sci. 16, 587, (1968).

[51]J. F. McKenzie, Planet. Space Sci. 18, 1, (1970).

[52]J. A. Fejer, Physics Fluids 6, 508, (1963).

[53]J. P. Heppner, N. F. Ness, C. S. Scearce, and T. L. Skillman, J. Geophys. Res. 68, 1, (1963).

[54]J. P. Heppner, M. Sugiura, T. L. Skillman, B. G. Ledley, and M. Campbell, J. Geophys. Res. 72, 5417, (1967).

[55]L. J. Cahill, Jr. and P. G. Amazeen, J. Geophys. Res. 68, 1835, (1963).

[56]H. S. Bridge, A. Egidi, A. Lazarus, E. Lyon, and L. Jacobson, in Space Research 5, edited by D. G. King-Hele et al. (North-Holland Publishing Co., Amsterdam, 1965).

[57]J. H. Wolfve, R. W. Silva, and M. A. Myers, J. Geophys. Res. 71, 1319, (1966).

[58]R. E. Holzer, M. G. McLead, and E. J. Smith, J. Geophys. Res. 71, 1481, (1966).

[59]J. R. Gosling, J. R. Asbridge, S. J. Bame, and I. B. Strong, J. Geophys. Res. 72, 101, (1967).

[60]L. J. Cahill, Jr. and V. L. Patel, Planet. Space Sci. 15, 997, (1967).

[61]B. U. Ö. Sonnerup and L. J. Cahill, Jr., J. Geophys. Res. 72, 171, (1967).

[62]B. U. Ö. Sonnerup and L. J. Cahill, Jr., J. Geophys. Res. 73, 1757, (1968).

[63]V. M. Vasyliunas, J. Geophys. Res. 73, 7519, (1968).

[64]M. Sugiura, T. L. Skillman, B. G. Ledley, and J. P. Heppner, in Earth's Particles and Fields, 1969, edited by B. M. McCormac (D. Reidel, Dordrecht, Holland, 1970).

[65]K. W. Ogilvie, M. Sugiura, and J. D. Scudder, J. Geophys. Res. 76, 3574, (1971).

[66]B. G. Ledley, J. Geophys. Res. 76, 6736, (1971).

[67]R. Simon, Astrophys. J. 128, 392, (1958).

[68]B. B. Kadomtsev, A. B. Mikhailovskii, and A. V. Timofeev, Soviet Phys. JETP 20, 1517, (1965).

[69]P. A. Sturrock, J. Appl. Phys. 31, 2052, (1960).

[70]P. A. Sturrock, in 6th Lockheed Symp. on Magnetohydrodynamics, Plasma Hydromagnetics, edited by D. Bershader (Stanford Univ. Press, Stanford, 1962).

[71]J. W. Miles, J. Acoust. Soc. Am. 29, 226, (1957).

[72]H. S. Ribner, J. Acous. Soc. Am. 29, 435, (1957).

[73]L. A. Frank, J. Geophys. Res. 72, 3753, (1967).

[74]C. P. Sonett and I. J. Abrams, J. Geophys. Res. 68, 1233, (1963).

[75]S. Olbert, A. Egidi, G. Moreno, and L. G. Pai, Trans. Amer. Geophys. Union 48, 177, (1967).

[76]R. E. Holtzer, M. G. McLead, and E. J. Smith, J. Geophys. Res. 71, (1966).